Acknowledgments

All authors acknowledge that the first two authors contributed equally to the study and are joint First Authors. This work was supported by Grants-in-Aid for Scientific Research from the Ministry of Health, Labour and Welfare of Japan, Grants-in-Aid for Scientific Research from the Ministry of Education, Culture, Sports, Science and Technology of Japan, a grant from Pharmaceuticals and Medical Devices Agency of Japan, and a grant from Japan Science and Technology Agency.

References

[1] M. Hirai, M. Koizumi, T. Hayakawa, H. Takahashi, S. Abe, H. Hirai, K. Miura, K. Inoue, Hierarchical map of protein unfolding and refolding at thermal equilibrium revealed by wide-angle X-ray scattering, Biochemistry 43 (2004) 9036–9049.

[2] Y. Yonezawa, S. Tanaka, T. Kubota, K. Wakabayashi, K. Yutani, S. Fujiwara, An insight into the pathway of the amyloid fibril formation of hen egg white lysozyme obtained from a small-angle X-ray and neutron scattering study, J. Mol. Biol. 323 (2002) 225–237.

[3] M. Hirai, H. Iwase, T. Hayakawa, K. Miura, K. Inoue, Structural hierarchy of several proteins observed by wide-angle solution scattering, J. Synchrotron Rad. 9 (2002) 202–205.

[4] M. Tehei, D. Madern, C. Pfister, G. Zacai, Fast dynamics of halophilic malate dehydrogenase and BSA measured by neutron scattering under various solvent conditions influencing protein stability, Proc. Natl. Acad. Sci. USA 98 (2001) 14356–14361.

[5] W.M. Garrison, Reaction mechanisms in the radiolysis of peptides, polypeptides, and proteins, Chem. Rev. 87 (1987) 381–389.

[6] S.D. Maleknia, C.Y. Ralston, M.D. Brenowitz, K.M. Downard, M.R. Chance, Millisecond radiolytic modification of peptides by synchrotron X-rays identified by mass spectrometry, Anal. Chem. 71 (1999) 3965–3973.

[7] G. Xu, M.R. Chance, Radiolytic modification of sulfur-containing amino acid residues in model peptides: fundamental studies for protein footprinting, Anal. Chem. 77 (2005) 2437–2449.

[8] S. Kuwamoto, S. Akiyama, T. Fujisawa, Radiation damage to a protein solution, detected by synchrotron X-ray small-angle scattering: dose-related considerations and suppression by cryoprotectant, J. Synchrotron Rad. 11 (2004) 462–468.

[9] F.F. Robert, D.J. Rodi, A. Mirza, T.C. Irving, E. Kondrashkinad, L. Makowski, High-resolution wide-angle X-ray scattering of protein solutions: effect of beam dose on protein integrity, J. Synchrotron Rad. 10 (2003) 398–404.

[10] F. Matumoto, K. Makiko, K. Maeda, H. Patzelt, Y. Maeda, S. Fujiwara, Conformational changes of troponin C within the thin filaments detected by neutron scattering, J. Mol. Biol. 342 (2002) 1209–1221.

[11] W. Yong, A. Lomakin, M.D. Kirkitadze, D.B. Teplow, S.-H. Chen, G.B. Benedek, Structure determination of micelle-like intermediates in amyloid-protein fibril assembly by using small angle neutron scattering, Proc. Natl. Acad. Sci. USA 99 (2002) 150–154.

[12] A.J. Doig, E. Hughes, R.M. Burke, T.J. Suã, R.K. Heenanå, J. Luã, Inhibition of toxicity and protofibril formation in the amyloid-β peptide β(25–35), Biochem. Soc. Trans. 30 (2002) 537–542.

[13] K. Lu, J. Jacob, P. Thiyagarajan, V.P. Conticello, D.G. Lynn, Exploiting amyloid fibril lamination for nanotube self-assembly, J. Am. Chem. Soc. 125 (2002) 6391–6393.

[14] K.D. Wilkinson, K.M. Lee, S. Deshpande, P. Duerksen-Hughes, J.M. Boss, J. Pohl, Ubiquitin and the Biology of the Cell, Plenum Press, New York, 1998, pp. 99–125.

[15] E. Leroy, R. Boyer, G. Auburger, B. Leube, G. Ulm, E. Mezey, G. Harta, M.J. Brownstein, S. Jonnalagada, T. Chernova, A. Dehejia, C. Lavedan, T. Gasser, P.J. Steinbach, K.D. Wilkinson, M.H. Polymeropoulos, The ubiquitin pathway in Parkinson's disease, Nature 395 (1998) 451–452.

[16] Y. Liu, H.A. Lashuel, A. Liu, P.T. Lansbury Jr., The UCH-L1 gene encodes two opposing enzymatic activities that affect a-synuclein degradation and Parkinson's disease susceptibility, Cell 111 (2002) 209–218.

[17] H. Osaka, Y.L. Wang, K. Takada, S. Takizawa, R. Setsuie, H. Li, Y. Sato, K. Nishikawa, Y.J. Sun, M. Sakurai, T. Harada, Y. Hara, I. Kimura, S. Chiba, K. Namikawa, H. Kiyama, M. Noda, S. Aoki, K. Wada, Ubiquitin carboxy-terminal hydrolase L1 binds to and stabilizes monoubiquitin ion neuron, Hum. Mol. Genet. 12 (2003) 1945–1958.

[18] Y. Manago, Y. Kanahori, A. Shimada, A. Sato, T. Amano, Y. Sato-Sano, R. Setsuie, M. Sakurai, S. Aoki, Y.-L. Wang, H. Osaka, K. Wada, M. Noda, Potentiation of ATP-induced currents due to activation of P2X receptors by ubiquitin carboxy-terminal hydrolase L1, J. Neurochem. 92 (2005) 1061–1072.

[19] D.M. Maraganore, M.J. Farrer, J.A. Hardy, S.J. Lincoln, S.K. McDonnell, W.A. Rocca, Case-control study of the ubiquitin carboxy-terminal hydrolase L1 gene in Parkinson s disease, Neurology 53 (1999) 1858–1860.

[20] P. Wintermeyer, R. Kruger, W. Kuhn, T. Muller, D. Woitalla, D. Berg, G. Becker, E. Leroy, M. Polymeropoulos, K. Berger, H. Przuntek, L. Schols, J.T. Epplen, O. Riess, Mutation analysis and association studies of the UCHL1 gene in German Parkinson's disease patients, Neuroreport 11 (2000) 2079–2082.

[21] J. Zhang, N. Hattori, E. Leroy, H.R. Morris, S. Kubo, T. Kobayashi, N.W. Wood, M.H. Polymeropoulos, Y. Mizuno, Association between a polymorphism of ubiquitin carboxyterminal hydrolase L1 (UCH-L1) gene and sporadic Parkinson's disease, Parkinsonism Relat. Disord. 6 (2000) 195–197.

[22] J. Satoh, Y. Kuroda, A polymorphic variation of serine to tyrosine at codon 18 in the ubiquitin C-terminal hydrolase-L1 gene is associated with a reduced risk of sporadic Parkinson's disease in a Japanese population, J. Neurol. Sci. 189 (2001) 113–117.

[23] Y. Momose, M. Murata, K. Kobayashi, M. Tachikawa, Y. Nakabayashi, I. Kanazawa, T. Toda, Association studies of multiple candidate genes for Parkinson s disease using single nucleotide polymorphisms, Ann. Neurol. 51 (2002) 133–136.

[24] K. Nishikawa, H. Li, R. Kawamura, H. Osaka, Y.L. Wang, Y. Hara, T. Hirokawa, Y. Manago, T. Amano, M. Noda, S. Aoki, K. Wada, Alterations of structure and hydrolase activity of parkinsonism-associated human ubiquitin carboxyl-terminal hydrolase L1 variants, Biochem. Biophys. Res. Commun. 304 (2003) 176–183.

[25] S.C. Johnston, C.N. Larsen, W.J. Cook, K.D. Wilkinson1, C.P. Hill, Crystal structure of a deubiquitinating enzyme (human UCH-L3) at 1.8 Å resolution, EMBO J. 16 (1997) 3787–3796.

[26] M.C. Peitsch, Protein modeling by E-mail, Bio/Technology 13 (1995) 658–660.

[27] N. Guex, M.C. Peitsch, SWISS-MODEL and the Swiss-Pdb Viewer: an environment for comparative protein modeling, Electrophoresis 18 (1997) 2714–2723.

[28] T. Schwede, J. Kopp, N. Guex, M.C. Peitsch, SWISS-MODEL: an automated protein homology-modeling server, Nucleic Acids Res. 31 (2003) 3381–3385.

[29] D.I. Svergun, C. Barberato, M.H.J. Koch, M. CRYSOL—a program to evaluate X-ray solution scattering of biological macromolecules from atomic coordinates, J. Appl. Crystallogr. 28 (1995) 768–773.

[30] D.I. Svergun, S. Richard, M.H.K. Koch, Z. Sayers, K.G. Zaccai, Protein hydration in solution: experimental observation by X-ray and neutron scattering, Proc. Natl. Acad. Sci. USA 95 (1998) 2267–2272.

[31] P. Debye, Zerstreuung von Rontgenstrahlen, Ann. Phys. 46 (1915) 809–823.

[32] J.T. Yang, C.S. Wu, H.M. Martinez, Calculation of protein conformation from circular dichroism, Methods Enzymol. 130 (1986) 208–269.

[33] R.H. Thomas, A.K. Roger, A.G. Margaret, F.G. John, O.F. Robert, Transfer of a b-turn structure to a new protein context, Nature 339 (1989) 73–76.

[34] A. Perezel, B.M. Foxman, G.D. Fasma, How reverse turns may mediate the formation of helical segments in proteins: an X-ray model, Proc. Natl. Acad. Sci. USA 89 (1992) 8210–8214.

Ubiquitin C-terminal hydrolase L1 regulates the morphology of neural progenitor cells and modulates their differentiation

Mikako Sakurai[1,2], Koichi Ayukawa[1], Rieko Setsuie[1,2], Kaori Nishikawa[1], Yoko Hara[1], Hiroki Ohashi[1,3], Mika Nishimoto[1,4], Toshiaki Abe[3], Yoshihisa Kudo[4], Masayuki Sekiguchi[1], Yae Sato[1,2], Shunsuke Aoki[1], Mami Noda[2] and Keiji Wada[1,*]

[1]Department of Degenerative Neurological Diseases, National Institute of Neuroscience, National Center of Neurology and Psychiatry, Kodaira, Tokyo, 187-8502, Japan
[2]Laboratory of Pathophysiology, Graduate School of Pharmaceutical Sciences, Kyushu University, Higashi-ku, Fukuoka, 812-8582, Japan
[3]Department of Neurosurgery, Graduate School of Medicine, Jikei University School of Medicine, Minato-ku, Tokyo, 105-8461, Japan
[4]Laboratory of Cellular Neurobiology, Tokyo University of Pharmacy and Life Science, Hachioji, Tokyo, 192-0392, Japan
*Author for correspondence (e-mail: wada@ncnp.go.jp)

Accepted 27 September 2005
Journal of Cell Science 119, 162-171 Published by The Company of Biologists 2006
doi:10.1242/jcs.02716

Summary

Ubiquitin C-terminal hydrolase L1 (UCH-L1) is a component of the ubiquitin system, which has a fundamental role in regulating various biological activities. However, the functional role of the ubiquitin system in neurogenesis is not known. Here we show that UCH-L1 regulates the morphology of neural progenitor cells (NPCs) and mediates neurogenesis. UCH-L1 was expressed in cultured NPCs as well as in embryonic brain. Its expression pattern in the ventricular zone (VZ) changed between embryonic day (E) 14 and E16, which corresponds to the transition from neurogenesis to gliogenesis. At E14, UCH-L1 was highly expressed in the ventricular zone, where neurogenesis actively occurs; whereas its expression was prominent in the cortical plate at E16. UCH-L1 was very weakly detected in the VZ at E16, which corresponds to the start of gliogenesis. In cultured proliferating NPCs, UCH-L1 was co-expressed with nestin, a marker of undifferentiated cells. In differentiating cells, UCH-L1 was highly co-expressed with the early neuronal marker TuJ1. Furthermore, when UCH-L1 was induced in nestin-positive progenitor cells, the number and length of cellular processes of the progenitors decreased, suggesting that the progenitor cells were differentiating. In addition, NPCs derived from *gad* (UCH-L1-deficient) mice had longer processes compared with controls. The ability of UCH-L1 to regulate the morphology of nestin-positive progenitors was dependent on its binding affinity for ubiquitin but not on hydrolase activity; this result was also confirmed using *gad*-mouse-derived NPCs. These results suggest that UCH-L1 spatially mediates and enhances neurogenesis in the embryonic brain by regulating progenitor cell morphology.

Key words: PGP9.5, UCH-L1, Nestin, Ubiquitin, Cell morphology, Differentiation, Progenitor

Introduction

Ubiquitin C-terminal hydrolase L1 (UCH-L1) is a member of the deubiquitylating enzymes and is one of the most abundant proteins in the brain. Whereas other UCH members are ubiquitously expressed, UCH-L1 is selectively expressed in neurons and testes/ovaries in the adult (Wilkinson et al., 1989). UCH-L1 is also known as PGP9.5 and is used as a neuron-specific marker in neuroanatomical and neuropathological studies (Dickson et al., 1994; McQuaid et al., 1995). Recent studies suggest that UCH-L1 is involved in neurodegeneration. The I93M mutation and the S18Y polymorphism in UCH-L1 are implicated in Parkinson's disease (Leroy et al., 1998; Satoh and Kuroda, 2001). Using gracile axonal dystrophy (*gad*) mice, we previously demonstrated that the dying-back type of axonal degeneration is caused by a deletion of the *Uchl1* gene (Saigoh et al., 1999). UCH-L1 has an affinity for ubiquitin and ensures its stability within neurons in vivo (Osaka et al., 2003). Furthermore, UCH-L1 has ubiquitin ligase activity (Liu et al., 2002). Thus, UCH-L1 might have multiple functions and more roles in biological phenomena than previously expected.

UCH-L1 mRNA is first detected at embryonic day (E) 8.5-9 in the neural tube and in the neural epithelium (Schofield et al., 1995). In addition, UCH-L1 immunoreactivity has been observed in the neural tube at E10.5 (Sekiguchi et al., 2003). However, its functional role in embryonic neurogenesis is not well understood. CDK5 and Dab1 are involved in regulating the migratory behavior of postmitotic neurons. Both p35, which is a CDK5 kinase, and Dab1 are degraded by the ubiquitin-proteasome pathway (Arnaud et al., 2003; Bock et al., 2004; Patrick et al., 1998). Thus, the ubiquitin system might be important in the migration and differentiation of postmitotic neurons and for the lamination pattern of the cerebral cortex.

Neural progenitor cells (NPCs) differentiate into neurons, astrocytes and oligodendrocytes (Qian et al., 1998; Qian et al., 2000; Shen et al., 1998). In the embryonic brain, neuroepithelial cells and radial glia are present in the ventricular zone (VZ); neurogenesis occurs first, followed by

gliogenesis. Committed progenitor cells move from the VZ to the cortical plate (CP) (Noctor et al., 2004). The differentiating cells migrate by means of radial migration, during which the migrating cells change their morphology (Kawauchi et al., 2003; Noctor et al., 2002; Tabata and Nakajima, 2003). Here, we analyzed the functional role of UCH-L1 using mouse embryonic NPCs. Our results indicate that UCH-L1 is expressed in nestin-positive NPCs and might regulate neurogenesis. The expression pattern of UCH-L1 changed in parallel with the transition from neuronal generation to glial generation. Furthermore, UCH-L1 modulated the length of nestin-positive processes in NPCs. Our results constitute the first evidence that UCH-L1 is important in neurogenesis and thus provide the basis for further investigation into the role of the ubiquitin system in neurogenesis.

Results

UCH-L1 expression in embryonic mouse brain

We first determined the specificity of the UCH-L1 antibody using immunoblotting (data not shown) and immunostaining. Because *gad* mice do not express endogenous UCH-L1 (Saigoh et al., 1999), we used these mice as a negative control. Heterozygous littermates had UCH-L1 immunostaining, whereas UCH-L1 immunoreactivity was not detected in the brains of *gad* mice (Fig. 1). These results confirmed the specificity of the antibody against UCH-L1. Using this antibody, we further compared the distribution and expression of UCH-L1 with the neural progenitor marker nestin and the early neuronal marker TuJ1. Nestin was expressed in the VZ of brains from both *gad* and heterozygous mice at E13 (Fig. 1). Nestin expression was observed throughout the region, whereas TuJ1 immunoreactivity was detected at the marginal zone (MZ). In heterozygous mice, UCH-L1 and nestin immunostaining overlapped in almost all cells in the VZ, suggesting that UCH-L1 is expressed in NPCs (Fig. 1A). TuJ1 expression colocalized with that of UCH-L1 in MZ cells, indicating that UCH-L1 is expressed in embryonic neurons as well (Fig. 1B). In E13 *gad* mouse brain, nestin staining differed compared with that in heterozygous littermates. Nestin staining was observed in many long radial fibers in the mutant, which we believed were radial glia; by contrast, staining in the heterozygotes occurred in radial glia as well as in neuronal cells at various stages of development (Fig. 1A; arrow and arrowhead).

We then looked for developmental changes in UCH-L1 expression. In the embryonic cerebral cortex, asymmetric cell division generates one neuron and one neural progenitor (Roegiers and Jan, 2004; Zhong et al., 1996; Zhong et al., 1997). These asymmetric cell divisions begin at E11, peak around E14, and subside after E16. At E14, astrocytes and oligodendrocytes are not yet present. However, at E16, glial cell production begins. The regional expression level for both nestin and TuJ1 did not change between E14 and E16 (Fig. 2A,B). At E14 and E16, nestin immunoreactivity was stronger in the VZ (Fig. 2A) and was faintly detected only along radial glial fibers in the CP (Fig. 2A,C; arrowhead) (Malatesta et al., 2003; Malatesta et al., 2000). TuJ1 immunoreactivity was predominantly detected in the MZ, CP, intermediate zone and subventricular zone at E14 and E16 (Fig. 2B,D). In the VZ, TuJ1 immunoreactivity was detected only in migrating neurons (Fig. 2D; arrowhead).

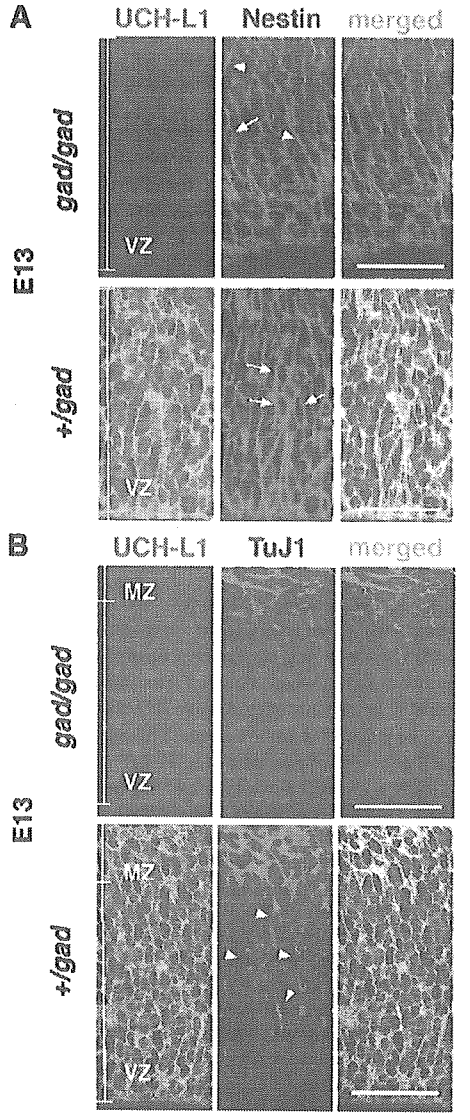

Fig. 1. Antibody specificity and expression of UCH-L1 in the ventricular zone at E13. UCH-L1 expression was detected using immunohistochemistry with anti-PGP9.5. UCH-L1 is not detected in the brain of *gad* mice at E13 (A,B) but is strongly expressed in heterozygous littermates (A,B). Confocal microscopic images of coronal sections of *gad* mice and heterozygous littermates were double stained with antibodies for the progenitor marker nestin and UCH-L1 (PGP9.5) (A) or for the early neuronal marker tubulin β III (TuJ1) and UCH-L1 (B). Long radial fibers are indicated by arrowheads, and various phases of progenitor cells are indicated by arrows (A). TuJ1-positive, migrating neuronal cells are indicated by arrowheads (B). MZ, marginal zone; VZ, ventricular zone. Bars, 40 μm.

By contrast, the pattern of UCH-L1 expression changed between E14 and E16 (Fig. 2A,B). At both stages of development, UCH-L1 was expressed in neuronal cells as well as in progenitor cells. UCH-L1 immunoreactivity was stronger in the VZ than in the CP at E14; however, the immunoreactivity

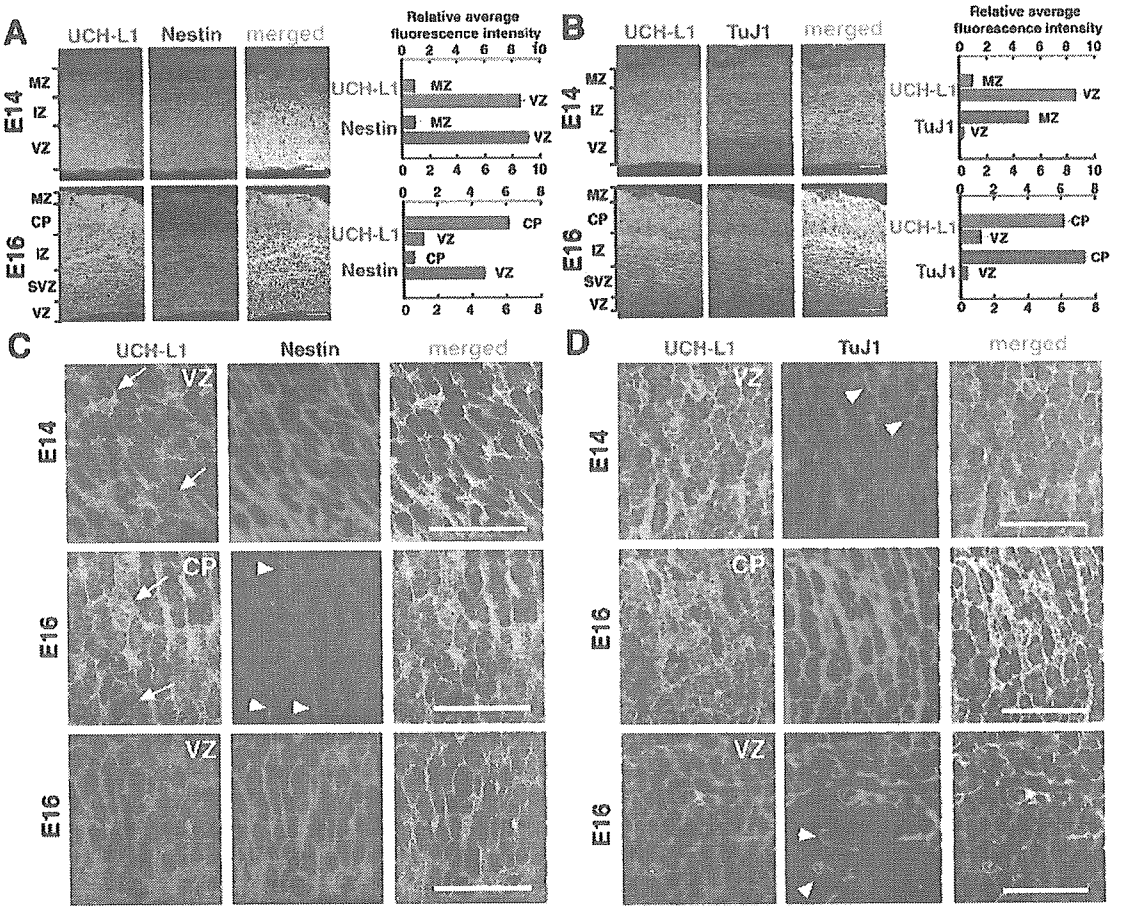

Fig. 2. Change in UCH-L1 expression pattern in the developing mouse brain. Cryosections of the brain at E14 and E16 were double stained with UCH-L1 and the neural progenitor marker nestin (A) or early neuronal marker TuJ1 (B). Unlike with UCH-L1, staining patterns for TuJ1 and nestin do not change between E14 and E16. At E14, UCH-L1 expression is higher in the VZ than in the MZ. At E16, higher expression of UCH-L1 is reciprocally detected in the CP. By contrast, at both E14 and E16, nestin is highly expressed in the VZ, and TuJ1 expression is higher in the MZ/CP. Fluorescence intensities per field (1700 μm^2) were measured in each layer of the E14 and E16 brain and are shown to the right. Bars, 80 μm. (C,D) Higher-magnification images from A,B of UCH-L1 expression in the E14 and E16 brain: UCH-L1 and nestin (C); UCH-L1 and TuJ1 (D). UCH-L1 and nestin are co-expressed in the VZ at E14 and E16. Nestin is expressed only in radial glial fibers (arrowheads) of the CP but not in neurons. UCH-L1 expression level is high. A representative cell with a high level of UCH-LI expression is indicated by a white arrow and one with low expression is indicated by a yellow arrow (C). An early neuronal marker, TuJ1, was expressed in both migrating (arrowheads) and mature neurons (D). CP, cortical plate; IZ, intermediate zone; MZ, marginal zone; SVZ, subventricular zone; VZ, ventricular zone. Bars, 40 μm.

was stronger in the CP than in the VZ at E16 (Fig. 2A,B). The regional change in UCH-L1 expression between E14 and E16 was further confirmed by measuring immunofluorescence intensities from confocal images of the MZ/CP and VZ. At E14, the relative UCH-L1 expression level in the VZ was 9.3 times higher than that in the MZ (Fig. 2A).

Conversely, at E16, when neuronal maturation occurs in the CP, UCH-L1 immunoreactivity in the CP was 5.0 times higher than in the VZ (Fig. 2B). UCH-L1 immunoreactivity colocalized with that of nestin in the VZ at both E14 and E16, although UCH-L1 expression in the VZ was lower at E16 (Fig. 2C). In the VZ at E14, nestin was expressed homogeneously; however, the pattern of UCH-L1 immunoreactivity was mixed, with strong and weak intensities (Fig. 2C; arrow). This expression pattern might reflect the heterogeneity of progenitor cells. Nestin-positive radial glial fibers were observed in the CP at E16 through mature neurons, which strongly expressed UCH-L1 (Fig. 2C) (Malatesta et al., 2000; Malatesta et al., 2003).

UCH-L1 and nestin expression in cultured NPCs

Because areas of nestin and UCH-L1 immunoreactivity overlapped in the VZ, where NPCs reside, we subsequently analyzed the transition of UCH-L1 expression using cultured NPCs. We performed double-labeling experiments for UCH-L1 and nestin expression in cultured NPCs. In the presence of basic fibroblast growth factor (bFGF), when NPCs are proliferating, the percentage of UCH-L1/nestin double-positive

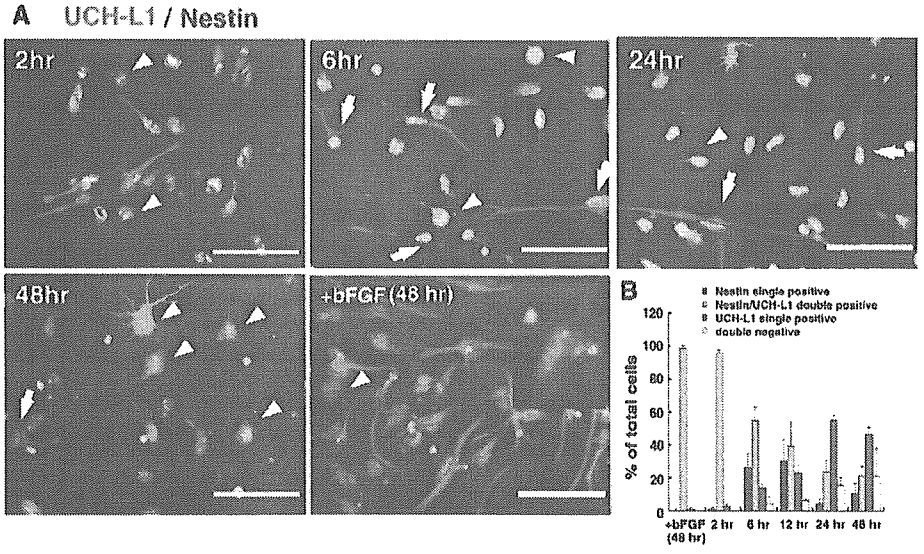

Fig. 3. Nestin and UCH-L1 expression in undifferentiated and differentiating NPCs at 2, 6, 12, 24 and 48 hours. (A) NPCs were immunolabeled with antibodies against nestin and UCH-L1 in the proliferating phase (+bFGF; at 48 hours) or the differentiation phase (–bFGF; 2, 6, 24, 48 hours). Cultures were counterlabeled with Hoechst nuclear dye to facilitate cell quantification. (B) Quantitative analysis of the percentage of cells stained with each antibody. Nestin-positive cells gradually decrease as differentiation proceeds. The UCH-L1 expression level is both high (arrowheads) and low (arrows) in nestin-positive cells at 6 hours. Each experiment was analyzed by counting cells in three independent wells at the indicated times. The experiments were repeated at least two times. Bars, 50 μm.

cells did not change 48 hours after plating, and almost all NPCs expressed UCH-L1 (Fig. 3A). The majority (97.5±2.2%; mean±s.d.) of cultured cells were nestin positive and most of them also stained for UCH-L1 2 hours after plating without bFGF, which triggers NPC differentiation. UCH-L1/nestin double-positive cells were detected at all time points, but as differentiation proceeded their numbers gradually decreased from 95.8±1.9% at 2 hours to 21.5±5.8% at 48 hours (Fig. 3A,B). Although UCH-L1 single-positive cells were rarely detected at 2 hours, the population increased with differentiation, and by 24 hours after bFGF removal 55.1±2.9% of cultured cells were UCH-L1 single-positive cells. Conversely, nestin single-positive cells were readily detected during the earlier phase of differentiation, especially at 6 hours (26.4±8.4% of total cells) and 12 hours (27.0±14.0% of total cells). The differentiating NPCs included nestin-positive cells in which UCH-L1 was either strongly or weakly expressed (Fig. 3A; arrow and arrowhead at 6 hours). These data indicate that UCH-L1 is expressed in progenitor cells as well as in differentiating NPCs. Nestin-positive cells can probably be

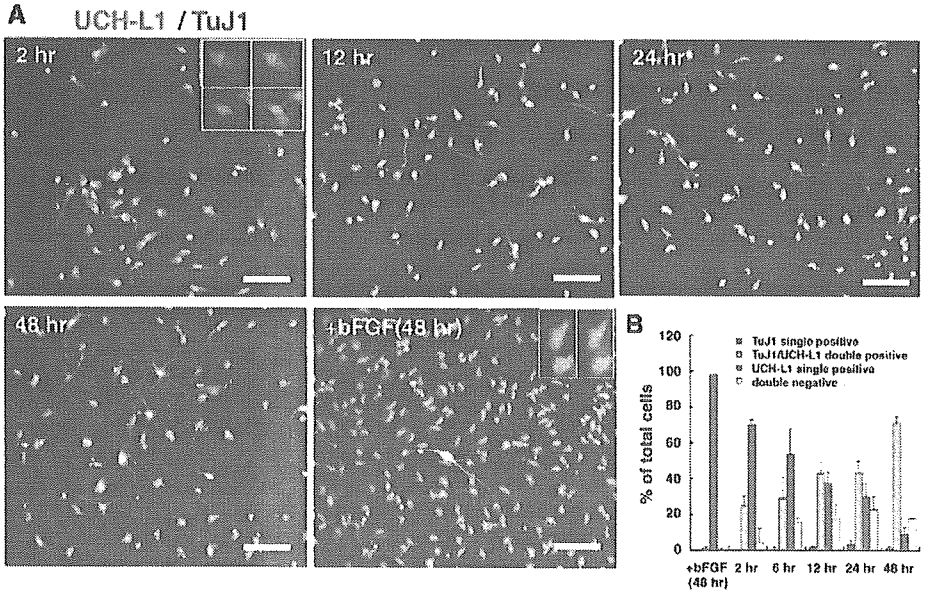

Fig. 4. UCH-L1 expression in neurogenesis. NPCs were immunolabeled with antibodies against TuJ1 and UCH-L1. Cultures were counterlabeled with Hoechst nuclear dye to facilitate cell quantification. Quantitative analysis of the percentage of cells stained with each antibody. (A) In the proliferating phase (+bFGF; at 48 hours) or the differentiation phase (–bFGF; 2, 12, 24, 48 hours), most TuJ1-positive cells co-express UCH-L1. The UCH-L1 expression level is both high and low in TuJ1-positive cells at 48 hours. (B) Quantitative analysis of the percentage of cells stained with each antibody. The number of TuJ1-positive cells gradually increased in the differentiating phase (–bFGF; B). Each experiment was analyzed by counting cells in three independent wells at the indicated times. The experiments were repeated at least two times. Bars, 50 μm.

categorized into at least two subgroups based on their UCH-L1 expression (Fig. 3A,B).

UCH-L1 and TuJ1 expression in cultured NPCs

We then analyzed the expression patterns of UCH-L1 and TuJ1. In the presence of bFGF, TuJ1-positive cells were rarely detected. However, in the absence of bFGF, TuJ1-positive cells were induced. In the cultures without bFGF, as the UCH-L1 single-positive cell population decreased with time, the UCH-L1/TuJ1 double-positive population increased (Fig. 4A,B). UCH-L1/TuJ1 double-negative cells were detected in the differentiating phases at 6, 12, 24 and 48 hours. UCH-L1/TuJ1 double-negative cells might be the nestin single-positive cells at 6 hours and 12 hours in Figs 3 and 4. TuJ1 single-positive cells were infrequently detected in the differentiating NPCs. Because 71.4±3.4% of NPCs differentiated into TuJ1-positive cells under our culture conditions without bFGF at 48 hours, almost all UCH-L1-positive cells are thought to differentiate into TuJ1-positive neuronal cells (Fig. 4A,B). The differentiating NPCs included TuJ1-positive cells in which UCH-L1 was either strongly or weakly expressed (Fig. 4A). These data indicate that UCH-L1-positive NPCs have a high potential for differentiating into neuronal cells and that TuJ1-positive neuronal cells are heterogeneous with regard to UCH-L1 expression.

Morphological classification of UCH-L1-positive NPCs

Nestin is a marker of undifferentiated cells, whereas UCH-L1 is a neuron-specific marker. Here, UCH-L1/nestin double-positive cells were present in cultured NPCs as well as in embryonic brain (Figs 2, 3). Cultured NPCs sequentially gave rise to neurons, then astrocytes, and finally oligodendrocytes (data not shown). Under our culture conditions, neurogenesis actively occurred in differentiating NPCs between 2 and 12 hours after plating (Fig. 4). Glial differentiation had not begun by this time. We collected differentiating NPCs at 6 hours and 12 hours after plating and then analyzed the morphology of nestin-positive cells (Fig. 5). Both UCH-L1/nestin double-positive cells and nestin single-positive cells were present in the population of differentiating NPCs. As the population of double-positive cells might represent a progression of differentiating neurons, we examined the morphology of these cells. Differentiating neurons undergo a stereotypical set of morphological changes, including length (from long to short) (Fukuda et al., 2003; Hartfuss et al., 2003; Nadarajah et al., 2001). We categorized the nestin-positive cells with respect to process length (long, short or round; Fig. 3). UCH-L1 single-positive and double-negative cells were included in the total number of cells. When the total length of processes was more than four times the diameter of the nucleus of the cell, the cell was categorized as 'long', whereas cells with shorter processes were categorized as 'short'. Cells that did not have processes were classified as 'round'. At 6 hours, the majority of nestin single-positive cells were long (18.2±7.6% vs 4.0±0.2% short cells; mean±s.d.; Fisher's PLSD, P=0.008), whereas the majority of UCH-L1/nestin double-positive cells were short (62.0±6.3%). This population was significantly greater than that of long cells (10.3±2.0%) and round cells (5.0±1.7%; Fisher's PLSD, P<0.0001). When NPCs with processes were subcategorized as unipolar, bipolar or multipolar, the unipolar population was significantly higher (62.3±16.9%) than the bipolar population (18.2±3.9%; Fisher's PLSD, P=0.002) in UCH-L1/nestin double-positive cells. Multipolar cells were not observed at 12 hours. However, in nestin single-positive cells, more NPCs were bipolar (16.5±4.6%) than unipolar (4.5±1.9%; Fisher's PLSD, P=0.009; Fig. 6B). Similar results were obtained at 12 hours (Fig. 6). Thus, most UCH-L1/nestin double-positive cells had shorter processes and were more likely to be unipolar.

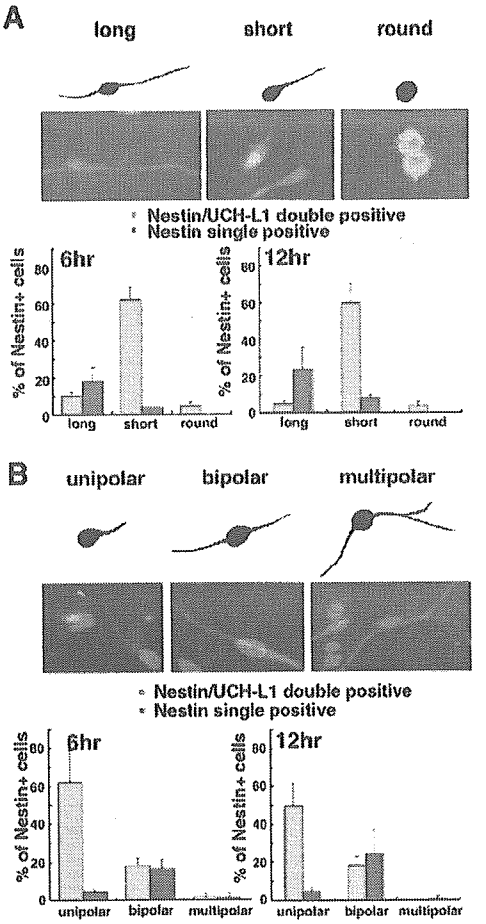

Fig. 5. Morphological identification of subpopulations of cultured NPCs at 6 and 12 hours after induction of differentiation. Differentiating NPCs were double stained with UCH-L1 and nestin. For the quantification depicted in A, differentiating NPCs stained with UCH-L1 and nestin were classified as long, short or round (see text). For the quantification depicted in B, differentiating NPCs were classified based on three kinds of cell morphology: unipolar, bipolar, or multipolar.

Effect of UCH-L1 on nestin-positive processes

We next examined the effect of UCH-L1 on proliferating NPC morphology using the transient transfection method. NPCs were allowed to proliferate for 48 hours after transfection and were then induced to differentiate for 12 hours. The cells were fixed, and the length of nestin-positive processes was examined. To quantify the relationship between UCH-L1 expression and process formation, we measured the total length

of nestin-positive processes. Untransfected NPCs that were nestin positive had mainly long, bipolar processes (Fig. 3A, +bFGF). Cells that were transfected with a green fluorescent protein (GFP) expression vector (negative control) had a morphology that was similar to that of untransfected cells (Fig. 6A). By contrast, cells transfected with wild-type (WT) UCH-L1 cDNA had significantly shorter processes (47.6±6.4 μm, mean±s.e.m., n=81) than mock-transfected cells (69.9±7.0 μm, n=82) (Fig. 6A).

We then examined the relationship between the UCH-L1 structure and its activity with respect to morphological induction. We prepared two UCH-L1 mutants: D30A UCH-L1 lacked hydrolase activity and binding affinity for ubiquitin (Fig. 6B,C) (Osaka et al., 2003); C90S UCH-L1 lacked hydrolase activity but maintained binding affinity for ubiquitin (Fig. 6B,C) (Osaka et al., 2003). We compared the deubiquitylating activity of each UCH-L1 mutant using Ub-AMC as a substrate. The D30A mutant had little hydrolase activity, and the activity of the C90S mutant was not detectable (Fig. 6B; right). Sodium dodecyl sulfate-polyacrylamide gel electrophoresis revealed that there were no detectable contaminating proteins in these recombinant protein preparations (Fig. 6B; left). Co-immunoprecipitation experiments demonstrated that WT UCH-L1 and the C90S mutant physically associated with monoubiquitin. The D30A mutant (as well as GFP alone, which was used as a control) did not associate with ubiquitin (Fig. 6C). Although we did not detect a statistically significant difference, cells transfected with the D30A mutant tended to have longer nestin-positive processes (83.4±7.1 μm, n=87) as compared with cells transfected with the GFP expression vector (Fig. 6A). By contrast, cells transfected with the C90S mutant had significantly shorter fibers (39.3±4.5 μm, n=120; ANOVA: F=11.5, P<0.0001; Dunnett's multiple comparison test: GFP vs WT, P<0.05; GFP vs C90S, P<0.001; GFP vs D30A, P>0.05; Fig. 6A). We also compared the length of nestin-positive processes among UCH-L1 mutants (Bonferroni-Dunn Multiple Comparison Test: WT vs C90S, P=0.32; WT vs D30A, P<0.0001; D30A vs C90S, P<0.0001). Taken together, our data suggest that the effect of UCH-L1 expression on NPC morphology is dependent on the interaction between monoubiquitin and UCH-L1.

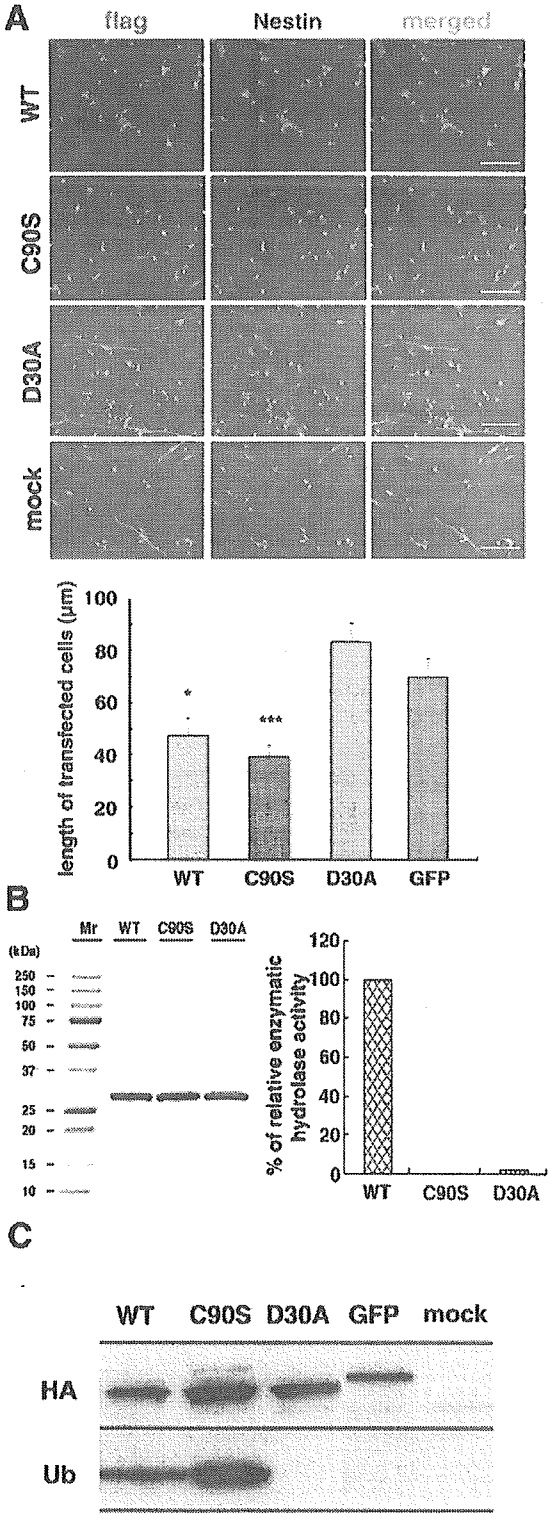

Fig. 6. The induction of short processes depends on the interaction between UCH-L1 and monoubiquitin. (A) FLAG-tagged WT UCH-L1, C90S UCH-L1, D30A UCH-L1 and GFP (all in the pCI-*neo* vector) were transfected into NPCs. Antibodies against the FLAG-tag were used to detect transfected UCH-L1. The green staining shows transfected cells and the red staining shows endogenous nestin. Transient transfection of each construct was performed under proliferating conditions. At 48 hours after transfection, bFGF was removed for 12 hours before the cultures were immunostained. The lengths of nestin-positive processes in immunostained cells were measured. Asterisks indicate differences from the value of GFP-transfected NPCs at *P<0.05 and ***P<0.001. Bars, 80 μm. (B) Visualization of recombinant 6HN-tagged UCH-L1 by sodium dodecyl sulfate-polyacrylamide gel electrophoresis with Coomassie staining (B, left). UCH-L1 hydrolase activity was measured by Ub-AMC hydrolysis. Enzyme concentration was 4.3 nM, and substrate concentration was 700 nM. Initial velocity data was used to determine the values for relative hydrolase activity of UCH-L1 (B, right). (C) UCH-L1 co-immunoprecipitated with Ub. Cytosolic extracts from NIH-3T3 cell lines stably expressing HA-tagged WT UCH-L1 and mutants thereof were immunoprecipitated using anti-HA and immunoblotted with anti-HA antibody or anti-Ub antibody.

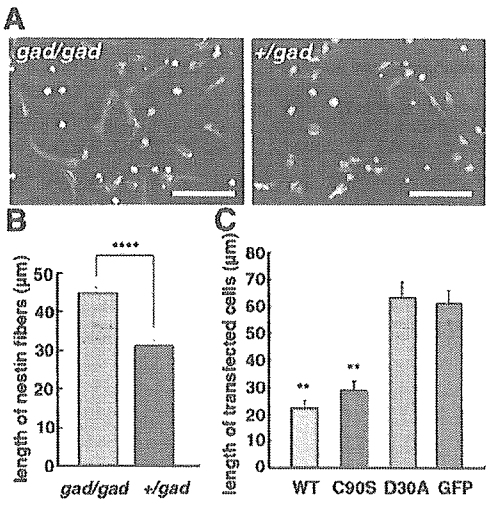

Fig. 7. A comparative experiment of *gad* mice and heterozygous littermates. The experiment compared *gad* mice (A,B) with a transfection study using FLAG-tagged WT UCH-L1, C90S UCH-L1, D30A UCH-L1 and GFP (mock) into *gad*-mouse-derived NPCs (C). The lengths of nestin-positive processes in immunostained cells were measured. NPCs from *gad* mice had longer nestin-positive processes compared with the control (A,B). (C) At 48 hours after transfection, bFGF was removed for 12 hours before the cultures were immunostained. The lengths of nestin-positive processes in immunostained cells were measured. Asterisks indicate differences from the value of GFP-transfected NPCs at $^{**}P<0.01$ and $^{****}P<0.0001$. Bar, 50 μm.

A comparative experiment using *gad*-mouse-derived NPCs

We did a comparative experiment using *gad* mice and heterozygous littermates. Nestin-positive NPCs from *gad* mice had longer processes. When we measured the length of nestin-positive fibers, NPCs from *gad* mice (45.0±1.4 μm, mean±s.e.m., n=366) had significantly longer nestin-positive processes compared with the control (31.4±1.3 μm, n=363) (Mann-Whitney U test: *gad* vs control, $P<0.0001$; Fig. 7A,B).

We next examined the effect of UCH-L1 on *gad*-mouse-derived NPCs using the transient transfection method. As observed in B6-derived cells, NPCs from *gad* mice that were transfected with WT UCH-L1 cDNA had significantly shorter processes (22.2±2.7 μm, mean±s.e.m., n=70) than mock-transfected cells (61.0±4.9 μm, n=88) (Bonferroni-Dunn multiple comparison test: GFP vs WT, $P<0.0001$) (Fig. 7C). Similarly, cells transfected with the C90S mutant had significantly shorter fibers (28.9±3.1 μm, n=71) (GFP vs C90S, $P<0.0001$). Although we did not detect a statistically significant difference, cells transfected with the D30A mutant tended to have longer nestin-positive processes (63.3±5.9 μm, n=80) as compared with cells transfected with the GFP expression vector (GFP vs D30A, P=0.70) (Fig. 7C). We also compared the length of nestin-positive processes among UCH-L1 mutants (Bonferroni-Dunn multiple comparison test: WT vs C90S, P=0.32; WT vs D30A, $P<0.0001$; D30A vs C90S, $P<0.0001$). Taken together, our data suggest that the effect of UCH-L1 expression on NPC morphology is dependent on the interaction between monoubiquitin and UCH-L1.

Discussion

UCH-L1 is a neuron-specific marker in the adult brain. In the present study, we provide experimental evidence that UCH-L1 is expressed in NPCs (Figs 2, 3). Using immunohistochemistry in the mouse brain, we detected UCH-L1 expression at E14 and E16. Interestingly, the expression pattern differed between E14 and E16 (Fig. 2). At E14, when the CP is forming, UCH-L1 expression was higher in the VZ than in the CP. At E14, the VZ contains progenitor cells that are generating neurons in the neocortex (Hashimoto and Mikoshiba, 2004; Malatesta et al., 2003). By contrast, UCH-L1 expression at E16 was lower in the VZ than in the CP. At E16, neuritogenesis and neuronal maturation are active in the CP, and gliogenesis is beginning in the VZ (Rice and Curran, 2001). The cerebral cortex layer becomes thicker at E16, where glial cells are not yet generated. The staining pattern for TuJ1 and nestin did not change between E14 and E16 (Fig. 2), indicating that UCH-L1 is highly expressed in the cortical layer prior to gliogenesis. The change in the expression pattern of UCH-L1 was coincident with the transition from neurogenesis to gliogenesis in the VZ. These results raise the possibility that UCH-L1 mediates not only the neuronal differentiation of NPCs but also the transition from neurogenesis to gliogenesis.

Time is a pivotal factor in the programmed sequence that produces neurons and glial cells from NPCs (Qian et al., 2000), in that the switch from neurogenesis to gliogenesis is regulated by time. The mechanism behind this progression of the progenitor cells is not well understood. Cultured NPCs generate neurons first, followed by astrocytes and then oligodendrocytes (Qian et al., 2000; Temple, 2001). This order of production for each population has been verified in vivo (Sauvageot and Stiles, 2002). The pattern of UCH-L1 immunoreactivity suggests that UCH-L1 is required for the onset of neurogenesis, which is followed by glial differentiation (Fig. 2).

We thus examined the role of UCH-L1 in neurogenesis using cultured NPCs. In UCH-L1/nestin double-staining experiments, the number of double-positive cells decreased with time in culture (Fig. 3). Conversely, UCH-L1 single-positive cells increased. In the double-staining experiments for UCH-L1 and TuJ1, the number of UCH-L1 single-positive cells decreased with time in culture, whereas the number of UCH-L1/TuJ1 double-positive cells increased (Fig. 4). These observations suggest that most UCH-L1-positive cells initially express nestin, but they express TuJ1 at a later stage. As we observed in vivo and in vitro (Figs 2-4), NPCs express UCH-L1, and its expression increases as the NPCs differentiate into neuronal cells. The number of nestin single-positive cells transiently increased before the UCH-L1 single-positive population increased (Fig. 3). The nestin single-positive population might have changed into the UCH-L1/nestin double-negative population (Fig. 3). Although the fate of the double-negative populations remains unknown, the double-negative cells might represent glial cells. Alternatively, some of the nestin single-positive cells might have changed into UCH-L1/nestin double-positive cells and then differentiated into UCH-L1 single-positive cells. A few UCH-L1-negative and TuJ1-positive cells were detected in the differentiating NPCs (Fig. 4). Thus, TuJ1-positive early neurons appear to be heterogeneous. UCH-L1/TuJ1 double-positive immunoreactivity suggested that UCH-L1 is not

absolutely required for some portion of neuronal cell development (Fig. 1B and Fig. 4A). This might explain why *gad* mouse neurons develop despite the absence of UCH-L1.

Because UCH-L1 was expressed in nestin-positive NPCs, we further examined the role of UCH-L1 in cell morphology (Fig. 5). Differentiating NPCs change morphology (Noctor et al., 2001), but the role of UCH-L1 in differentiating neurons has not been investigated. We classified nestin-positive cells based on the length of their processes. Nestin single-positive cells were predominantly long, whereas most UCH-L1/nestin double-positive cells were predominantly short (Fig. 5). These results suggest that UCH-L1 plays a role in regulating NPC process length. We examined this possibility by inducing UCH-L1 in nestin-positive cells. Untransfected, proliferating nestin-positive NPCs had mainly long and bipolar processes [Fig. 3A, bFGF (48 hours)], but when UCH-L1 was transfected, the length of nestin-positive NPC processes shortened (Fig. 6A). The unipolar population increased following UCH-L1 expression. These results support the idea that UCH-L1 regulates NPC morphology. This idea was further confirmed by observations in NPCs from *gad* mice; as shown in Fig. 7B, NPCs from homozygous *gad* mice had longer processes than those from heterozygous controls. In addition, we observed that transfection of UCH-L1 shortened the processes of NPCs from *gad* mice compared with mock transfectants (Fig. 7C).

Our results also suggest that at least two populations of NPCs exist in the embryonic brain. The populations can be classified by the presence or absence of UCH-L1. In the dentate gyrus of the adult mouse brain, there are two distinct subpopulations of nestin-positive cells (Fukuda et al., 2003): those having short processes differentiate into neurons, whereas those having long processes generate late progenitors, which have short processes. The nestin staining pattern of brains from *gad* mice differed from that of brains from heterozygous littermates (Fig. 1). In the *gad* mouse brain, nestin-positive radial fibers were prominent, and almost all progenitor cells appeared to have long processes (Fig. 1). Since UCH-L1 affected NPC morphology (Fig. 6A and Fig. 7C), the difference in vivo indicates that differentiation itself was modulated by the absence of UCH-L1. Considering that neurons are present in the *gad* mouse even though it lacks UCH-L1 expression, further investigation into the morphological role of UCH-L1 using various approaches including the BrdU studies should provide important information about the heterogeneity of cortical neurons.

UCHs hydrolyze ubiquitin C-terminal small adducts in vitro (Larsen et al., 1998). Recently, a significant relationship was reported between UCH-L1 hydrolase activity and cell proliferation in lung cancer cell lines (Liu et al., 2003). We previously demonstrated that UCH-L1 extends ubiquitin half-life and prevents ubiquitin degradation. This function depends on the interaction between UCH-L1 and monoubiquitin but not on hydrolase activity (Osaka et al., 2003). In the present study, WT UCH-L1 and the C90S mutant both decreased the length of NPC processes. Both molecules associate with monoubiquitin, unlike another mutant, D30A, which did not affect process length (Fig. 6). Similar results were obtained from the transfection study using nestin-positive NPCs from *gad* mice (Fig. 7C). Thus, the effect of UCH-L1 on NPC process length is dependent on the interaction between UCH-L1 and ubiquitin but not on hydrolase activity. Although we did not examine the ligase activity of each mutant (Liu et al., 2002), the C90S mutant is unlikely to have ligase activity, because conjugation of ubiquitin to the C90S mutant forms a stable complex that prevents the release of ubiquitin (Sullivan and Vierstra, 1993). This observation suggests that the ligase activity is not related to the morphological changes that occurred in NPCs.

The ubiquitin system has an essential role in various physiological events, including cell-cycle progression, specific gene transcription, membrane protein trafficking, reversal of stress damage and intracellular signaling (Weissman, 2001). In cortical neurogenesis, the role of the ubiquitin system is not well understood. Several molecules that are important in cortical neurogenesis, including Notch, P35 and Dab1, are ubiquitylated (Arnaud et al., 2003; Bock et al., 2004; Patrick et al., 1998; Qiu et al., 2000). Here we show for the first time that UCH-L1 is expressed in NPCs and regulates their morphology. In addition, in vivo UCH-L1 expression is localized to the VZ and cortical layers that are undergoing neurogenesis. Cells undergoing gliogenesis had little UCH-L1 expression in vivo. These results suggest that UCH-L1 facilitates neurogenesis, an activity that appears to depend on the affinity of UCH-L1 for ubiquitin.

Materials and Methods

Animals

Pregnant C57BL/6J mice were purchased from CLEA Japan. The *gad* mouse is an autosomal recessive mutant that was obtained by crossing CBA and RFM mice (Saigoh et al., 1999). The *gad* line was maintained by intercrossing for more than 20 generations (Kwon et al., 2003; Saigoh et al., 1999). All animal experiments were performed in the laboratory according to the NIH Standards for Treatment of Laboratory Animals.

Antibodies and reagents

Monoclonal and polyclonal antibodies used in this study were as follows: monoclonal anti-nestin antibody (Becton Dickinson; and Rat401, Developmental Studies Hybridoma Bank, The University of Iowa, Iowa City, IA), monoclonal anti-neuronal tubulin β III antibody (TuJ1; Covance), polyclonal anti-UCH-L1 antibody (PGP9.5; RA95101, UltraClone), and polyclonal anti-FLAG antibody (Sigma). All secondary polyclonal antibodies conjugated to Alexa Fluor fluorescein were purchased from Molecular Probes.

Cortical NPC culture and differentiation conditions in C57BL/6 mice

Cortical NPCs were cultured as previously described (Nakashima et al., 1999). Briefly, embryos were removed from pregnant C57BL/6J mice (CLEA Japan) and staged according to morphological criteria to confirm the gestational day (Kaufman et al., 1998). Developing mouse cerebral cortex was dissected from E14 embryos. Cells were mechanically dissociated by trituration and plated at a concentration of 3.0×10^6 cells per 10 cm dish (Becton Dickinson) precoated with 10 ml of 15 μg/ml poly-L-ornithine (Sigma) and 10 ml of 1 μg/ml fibronectin (Nitta Gelatin). Cells were expanded for 5 days in serum-free neurobasal (NB) medium (Invitrogen) supplemented with B27 (Invitrogen), 0.5 mM L-glutamine (Invitrogen), 100 U/ml penicillin and 100 μg/ml streptomycin (Invitrogen). This medium contained 10 ng/ml bFGF (PeproTech). Cultures were maintained at 37°C in an atmosphere of 95% air and 5% CO_2. For secondary culture, bFGF-expanded NPCs were washed in warm Hank's Balanced Salt Solution, detached with mechanical pipetting, and resuspended in NB medium supplemented with B27, but not bFGF. Cells were then replated in 24-well plates (Nunc; 1.8×10^5 cells per well) that were precoated with 500 μl of 15 μg/ml poly-L-ornithine and 500 μl of 1 μg/ml fibronectin for immunofluorescence staining at each time point.

Cortical NPC culture and differentiation conditions in *gad* mice

Culture of NPCs derived from *gad* mice was performed as with NPCs derived from B6 mice. Developing mouse cerebral cortex was dissected from embryos at E13.5 to E14.5. The precise gestational day was determined according to previously established morphological criteria (Kaufman et al., 1998). NPCs from each embryo were collected and cultured separately. Each genotype was determined later using PCR and, as a result, each pair of *gad* and control littermate mice from two sets of

parents were used. Each culture of NPCs was replated in 24-well plates without bFGF and stained using anti-UCH-L1 24 hours after plating.

Immunohistochemistry

Brain sections were stained as previously described (Li et al., 2003; Osaka et al., 2003). Briefly, E14 and E16 mouse brains were removed and fixed in 4% paraformaldehyde/phosphate-buffered saline (PBS) for 2 hours at room temperature, cryoprotected in 30% sucrose in PBS and frozen in dry ice. Sections (20 μm thick) were cut on a cryostat, and mounted on aminopropylsilane (APS)-coated glass slides. They were then washed three times in PBS for 5 minutes, and blocked for 1 hour at room temperature with 3% bovine serum albumin, 2% (v/v) normal goat serum, and 0.2% (v/v) Triton X-100 in PBS (pH 7.4). Sections were incubated with primary antibodies [anti-nestin antibody (Rat-401) 1:10; or anti-UCH-L1 antibody (RA95101) 1:4000; or anti-TuJ1 antibody, 1:1000] overnight at 4°C or for 2 hours at room temperature. After rinsing in PBS, the sections were incubated for 2 hours with diluted fluorescein-conjugated secondary antibody (1:200). The images were obtained with a confocal laser scanning TCS SL microscope, and detailed analyses were performed using an LSC confocal microscope system (Leica). Immunofluorescence intensities were measured from confocal images with Mac SCOPE software (version 2.59; Mitani).

Immunocytochemistry

Cells were stained as previously described (Aoki et al., 2002). Briefly, all incubations and washes were performed at room temperature. Cells were fixed with 3.8% formaldehyde/PBS for 10 minutes and permeabilized with 0.02% (v/v) Triton X-100/PBS for 5 minutes. Fixed cells were blocked with 3.3% goat serum for 30 minutes. Cells were incubated with a diluted primary polyclonal or monoclonal antibody (both were used for double staining) for 0.5-1 hour. The cells were then incubated with diluted secondary antibody conjugated to fluorescein for 0.5-1 hour. Antibody dilutions were as follows: anti-UCH-L1 antibody, 1:4000; anti-nestin antibody, 1:500; anti-TuJ1, 1:500. All secondary antibodies were diluted 1:200 in 1% goat serum/PBS before use. The images were obtained with fluorescence microscopy on an IX70 microscope (Olympus).

Transfection

For C57BL/6 mice, cells replated in 24-well plates were cultured overnight in growth medium containing bFGF and B27. The next day, each construct was transfected using Lipofectamine 2000 (Invitrogen) according to the manufacturer's instructions. NPCs were allowed to proliferate for 48 hours after transfection and then induced to differentiate for 12 hours without bFGF. For *gad*-mouse-derived NPCs, transfection was done in a similar manner.

Expression plasmids for human UCH-L1 variants

Mutant cDNAs encoding human UCH-L1 containing either the D30A or C90S substitution were obtained using the QuikChange site-directed mutagenesis kit (Stratagene) with the following mutagenesis oligonucleotides: 5′-CAGTGG-CGCTTCGTGGCCGTGCTGGGGCTGGAAG-3′ and 5′-CTTCCAGCCCCAG-CACGGCCACGAAGCGCCACTG-3′ for D30A; 5′-CCATTGGGAATTCCTCT-GGCACAATCGGAC-3′ and 5′-GTCCGATTGTGCCACAGGAATTCCCAA-TGG-3′ for C90S. Each single-nucleotide mutation in the resulting plasmids was confirmed by sequencing. Mammalian expression plasmids containing either FLAG-tagged human WT UCH-L1 or the D30A or C90S mutants were constructed using a pCI-*neo* mammalian expression vector (Promega). Bacterial expression plasmids containing either 6HN-tagged human WT UCH-L1 or the D30A or C90S mutants were constructed using a tetracycline-inducible expression system. *Xho*I-*Not*I cDNA fragments of the pCI-*neo* WT UCH-L1 or the D30A and C90S mutants and constructs were digested, and the DNA fragments were ligated between the *Sal*I and *Not*I sites in pPROtetE233 (Clontech) to generate pPROtetE233 6HN-tagged human WT, D30A and C90S UCH-L1 vectors. These expression plasmids were confirmed by sequencing.

In vitro assay for human UCH-L1 activity

Purified human UCH-L1 and the fluorogenic substrate ubiquitin-7-amino-4-methylcoumarin (Ub-AMC; Boston Biochem) were used to determine steady-state kinetic parameters as described previously (Nishikawa et al., 2003).

Immunoprecipitation

NIH-3T3 cells stably expressing human WT UCH-L1 or the C90S or D30A mutants, all with an HA-FLAG double tag at the N terminus, were cultured to subconfluency in a 10 cm dish, lyzed with 1 ml of modified RIPA buffer [50 mM Tris-HCl, pH 7.5, 1% (v/v) NP-40, 0.25% sodium deoxycholate, 150 mM NaCl, 1 mM EDTA] with EDTA-free complete protease inhibitor cocktail (Roche), sonicated and centrifuged at 18,000 *g* for 20 minutes at 4°C. Immunoprecipitation was performed as described previously (Ogawa et al., 2002).

Statistics

Statistical analyses were performed using StatView, version 5.0 (SAS) and Prism, version 3 (GraphPad Software). Analysis of variance (ANOVA) was used to assess differences between groups. A P value of less than 0.05 was considered statistically significant. When ANOVA results were statistically significant, they were examined by Fisher's PLSD, or Dunnett's multiple comparison test, or Bonferroni-Dunn multiple comparisons post hoc test. Differences between *gad* mice and control mice were analyzed using the Mann-Whitney U test.

The authors thank Yuh Nung Jan and Hua-Shun Li for providing the immunohistochemistry methods; Yoshihiro Nakatani and Hidesato Ogawa for providing the retroviral expression system and immunoprecipitation methods; and Masako Shikama for the care and breeding of animals. This work was supported by Grants-in-Aid for Scientific Research from the Ministry of Health, Labour and Welfare of Japan, and Grants-in-Aid for Scientific Research from the Ministry of Education, Culture, Sports, Science and Technology of Japan.

References

Aoki, S., Su, Q., Li, H., Nishikawa, K., Ayukawa, K., Hara, Y., Namikawa, K., Kiryu-Seo, S., Kiyama, H. and Wada, K. (2002). Identification of an axotomy-induced glycosylated protein, AIGP1, possibly involved in cell death triggered by endoplasmic reticulum-Golgi stress. *J. Neurosci.* **22**, 10751-10760.

Arnaud, L., Ballif, B. A. and Cooper, J. A. (2003). Regulation of protein tyrosine kinase signaling by substrate degradation during brain development. *Mol. Cell. Biol.* **23**, 9293-9302.

Bock, H. H., Jossin, Y., May, P., Bergner, O. and Herz, J. (2004). Apolipoprotein E receptors are required for reelin-induced proteasomal degradation of the neuronal adaptor protein Disabled-1. *J. Biol. Chem.* **279**, 33471-33479.

Dickson, D. W., Schmidt, M. L., Lee, V. M., Zhao, M. L., Yen, S. H. and Trojanowski, J. Q. (1994). Immunoreactivity profile of hippocampal CA2/3 neurites in diffuse Lewy body disease. *Acta Neuropathol. (Berl.)* **87**, 269-276.

Fukuda, S., Kato, F., Tozuka, Y., Yamaguchi, M., Miyamoto, Y. and Hisatsune, T. (2003). Two distinct subpopulations of nestin-positive cells in adult mouse dentate gyrus. *J. Neurosci.* **23**, 9357-9366.

Hartfuss, E., Forster, E., Bock, H. H., Hack, M. A., Leprince, P., Luque, J. M., Herz, J., Frotscher, M. and Gotz, M. (2003). Reelin signaling directly affects radial glia morphology and biochemical maturation. *Development* **130**, 4597-4609.

Hashimoto, M. and Mikoshiba, K. (2004). Neuronal birthdate-specific gene transfer with adenoviral vectors. *J. Neurosci.* **24**, 286-296.

Kaufman, M. H., Brune, R. M., Davidson, D. R. and Baldock, R. A. (1998). Computer-generated three-dimensional reconstructions of serially sectioned mouse embryos. *J. Anat.* **193**, 323-336.

Kawauchi, T., Chihama, K., Nabeshima, Y. and Hoshino, M. (2003). The in vivo roles of STEF/Tiam1, Rac1 and JNK in cortical neuronal migration. *EMBO J.* **22**, 4190-4201.

Kwon, J., Kikuchi, T., Setsuie, R., Ishii, Y., Kyuwa, S. and Yoshikawa, Y. (2003). Characterization of the testis in congenitally ubiquitin carboxy-terminal hydrolase-1 (Uch-L1) defective (gad) mice. *Exp. Anim.* **52**, 1-9.

Larsen, C. N., Krantz, B. A. and Wilkinson, K. D. (1998). Substrate specificity of deubiquitinating enzymes: ubiquitin C-terminal hydrolases. *Biochemistry* **37**, 3358-3368.

Leroy, E., Boyer, R., Auburger, G., Leube, B., Ulm, G., Mezey, E., Harta, G., Brownstein, M. J., Jonnalagada, S., Chernova, T. et al. (1998). The ubiquitin pathway in Parkinson's disease. *Nature* **395**, 451-452.

Li, H. S., Wang, D., Shen, Q., Schonemann, M. D., Gorski, J. A., Jones, K. R., Temple, S., Jan, L. Y. and Jan, Y. N. (2003). Inactivation of Numb and Numblike in embryonic dorsal forebrain impairs neurogenesis and disrupts cortical morphogenesis. *Neuron* **40**, 1105-1118.

Liu, Y., Fallon, L., Lashuel, H. A., Liu, Z. and Lansbury, P. T., Jr (2002). The UCH-L1 gene encodes two opposing enzymatic activities that affect alpha-synuclein degradation and Parkinson's disease susceptibility. *Cell* **111**, 209-218.

Liu, Y., Lashuel, H. A., Choi, S., Xing, X., Case, A., Ni, J., Yeh, L. A., Cuny, G. D., Stein, R. L. and Lansbury, P. T., Jr (2003). Discovery of inhibitors that elucidate the role of UCH-L1 activity in the H1299 lung cancer cell line. *Chem. Biol.* **10**, 837-846.

Malatesta, P., Hartfuss, E. and Gotz, M. (2000). Isolation of radial glial cells by fluorescent-activated cell sorting reveals a neuronal lineage. *Development* **127**, 5253-5263.

Malatesta, P., Hack, M. A., Hartfuss, E., Kettenmann, H., Klinkert, W., Kirchhoff, F. and Gotz, M. (2003). Neuronal or glial progeny: regional differences in radial glia fate. *Neuron* **37**, 751-764.

McQuaid, S., McConnell, R., McMahon, J. and Herron, B. (1995). Microwave antigen retrieval for immunocytochemistry on formalin-fixed, paraffin-embedded post-mortem CNS tissue. *J. Pathol.* **176**, 207-216.

Nadarajah, B., Brunstrom, J. E., Grutzendler, J., Wong, R. O. and Pearlman, A. L. (2001). Two modes of radial migration in early development of the cerebral cortex. *Nat. Neurosci.* **4**, 143-150.

Nakashima, K., Yanagisawa, M., Arakawa, H., Kimura, N., Hisatsune, T., Kawabata, M., Miyazono, K. and Taga, T. (1999). Synergistic signaling in fetal brain by STAT3-Smad1 complex bridged by p300. *Science* **284**, 479-482.

Nishikawa, K., Li, H., Kawamura, R., Osaka, H., Wang, Y. L., Hara, Y., Hirokawa, T., Manago, Y., Amano, T., Noda, M. et al. (2003). Alterations of structure and

hydrolase activity of parkinsonism-associated human ubiquitin carboxyl-terminal hydrolase L1 variants. *Biochem. Biophys. Res. Commun.* **304**, 176-183.

Noctor, S. C., Flint, A. C., Weissman, T. A., Dammerman, R. S. and Kriegstein, A. R. (2001). Neurons derived from radial glial cells establish radial units in neocortex. *Nature* **409**, 714-720.

Noctor, S. C., Flint, A. C., Weissman, T. A., Wong, W. S., Clinton, B. K. and Kriegstein, A. R. (2002). Dividing precursor cells of the embryonic cortical ventricular zone have morphological and molecular characteristics of radial glia. *J. Neurosci.* **22**, 3161-3173.

Noctor, S. C., Martinez-Cerdeno, V., Ivic, L. and Kriegstein, A. R. (2004). Cortical neurons arise in symmetric and asymmetric division zones and migrate through specific phases. *Nat. Neurosci.* **7**, 136-144.

Ogawa, H., Ishiguro, K., Gaubatz, S., Livingston, D. M. and Nakatani, Y. (2002). A complex with chromatin modifiers that occupies E2F- and Myc-responsive genes in G0 cells. *Science* **296**, 1132-1136.

Osaka, H., Wang, Y. L., Takada, K., Takizawa, S., Setsuie, R., Li, H., Sato, Y., Nishikawa, K., Sun, Y. J., Sakurai, M. et al. (2003). Ubiquitin carboxy-terminal hydrolase L1 binds to and stabilizes monoubiquitin in neuron. *Hum. Mol. Genet.* **12**, 1945-1958.

Patrick, G. N., Zhou, P., Kwon, Y. T., Howley, P. M. and Tsai, L. H. (1998). p35, the neuronal-specific activator of cyclin-dependent kinase 5 (Cdk5) is degraded by the ubiquitin-proteasome pathway. *J. Biol. Chem.* **273**, 24057-24064.

Qian, X., Goderie, S. K., Shen, Q., Stern, J. H. and Temple, S. (1998). Intrinsic programs of patterned cell lineages in isolated vertebrate CNS ventricular zone cells. *Development* **125**, 3143-3152.

Qian, X., Shen, Q., Goderie, S. K., He, W., Capela, A., Davis, A. A. and Temple, S. (2000). Timing of CNS cell generation: a programmed sequence of neuron and glial cell production from isolated murine cortical stem cells. *Neuron* **28**, 69-80.

Qiu, L., Joazeiro, C., Fang, N., Wang, H. Y., Elly, C., Altman, Y., Fang, D., Hunter, T. and Liu, Y. C. (2000). Recognition and ubiquitination of Notch by Itch, a hect-type E3 ubiquitin ligase. *J. Biol. Chem.* **275**, 35734-35737.

Rice, D. S. and Curran, T. (2001). Role of the reelin signaling pathway in central nervous system development. *Annu. Rev. Neurosci.* **24**, 1005-1039.

Roegiers, F. and Jan, Y. N. (2004). Asymmetric cell division. *Curr. Opin. Cell Biol.* **16**, 195-205.

Saigoh, K., Wang, Y. L., Suh, J. G., Yamanishi, T., Sakai, Y., Kiyosawa, H., Harada, T., Ichihara, N., Wakana, S., Kikuchi, T. et al. (1999). Intragenic deletion in the gene encoding ubiquitin carboxy-terminal hydrolase in gad mice. *Nat. Genet.* **23**, 47-51.

Satoh, J. and Kuroda, Y. (2001). A polymorphic variation of serine to tyrosine at codon 18 in the ubiquitin C-terminal hydrolase-L1 gene is associated with a reduced risk of sporadic Parkinson's disease in a Japanese population. *J. Neurol. Sci.* **189**, 113-117.

Sauvageot, C. M. and Stiles, C. D. (2002). Molecular mechanisms controlling cortical gliogenesis. *Curr. Opin. Neurobiol.* **12**, 244-249.

Schofield, J. N., Day, I. N., Thompson, R. J. and Edwards, Y. H. (1995). PGP9.5, a ubiquitin C-terminal hydrolase; pattern of mRNA and protein expression during neural development in the mouse. *Brain Res. Dev. Brain Res.* **85**, 229-238.

Sekiguchi, S., Yoshikawa, Y., Tanaka, S., Kwon, J., Ishii, Y., Kyuwa, S., Wada, K., Nakamura, S. and Takahashi, K. (2003). Immunohistochemical analysis of protein gene product 9.5, a ubiquitin carboxyl-terminal hydrolase, during placental and embryonic development in the mouse. *Exp. Anim.* **52**, 365-369.

Shen, Q., Qian, X., Capela, A. and Temple, S. (1998). Stem cells in the embryonic cerebral cortex: their role in histogenesis and patterning. *J. Neurobiol.* **36**, 162-174.

Sullivan, M. L. and Vierstra, R. D. (1993). Formation of a stable adduct between ubiquitin and the Arabidopsis ubiquitin-conjugating enzyme, AtUBC1+. *J. Biol. Chem.* **268**, 8777-8780.

Tabata, H. and Nakajima, K. (2003). Multipolar migration: the third mode of radial neuronal migration in the developing cerebral cortex. *J. Neurosci.* **23**, 9996-10001.

Temple, S. (2001). The development of neural stem cells. *Nature* **414**, 112-117.

Weissman, A. M. (2001). Themes and variations on ubiquitylation. *Nat. Rev. Mol. Cell. Biol.* **2**, 169-178.

Wilkinson, K. D., Lee, K. M., Deshpande, S., Duerksen-Hughes, P., Boss, J. M. and Pohl, J. (1989). The neuron-specific protein PGP 9.5 is a ubiquitin carboxyl-terminal hydrolase. *Science* **246**, 670-673.

Zhong, W., Feder, J. N., Jiang, M. M., Jan, L. Y. and Jan, Y. N. (1996). Asymmetric localization of a mammalian numb homolog during mouse cortical neurogenesis. *Neuron* **17**, 43-53.

Zhong, W., Jiang, M. M., Weinmaster, G., Jan, L. Y. and Jan, Y. N. (1997). Differential expression of mammalian Numb, Numblike and Notch1 suggests distinct roles during mouse cortical neurogenesis. *Development* **124**, 1887-1897.

Exp. Anim. 55(1), 35–43, 2006

The Region-Specific Functions of Two Ubiquitin C-Terminal Hydrolase Isozymes along the Epididymis

Jungkee KWON[1, 3], Satoshi SEKIGUCHI[2], Yu-Lai WANG[1], Rieko SETSUIE[1], Yasuhiro YOSHIKAWA[2], and Keiji WADA[1]

[1]*Department of Degenerative Neurological Diseases, National Institute of Neuroscience, National Center of Neurology and Psychiatry, 4–1–1 Ogawahigashi, Kodaira, Tokyo 187-8502,*
[2]*Department of Biomedical Science, Graduate School of Agricultural and Life Sciences, The University of Tokyo, 1–1–1 Yayoi, Bunkyo-ku, Tokyo 113-8657, Japan, and*
[3]*Laboratory of Animal Medicine, College of Veterinary Medicine, Chonbuk National University, 664–14 Duckjin-Ku, Jeonju 561-756, Korea*

Abstract: *We previously showed that* gad *mice, which are deficient for ubiquitin C-terminal hydrolase L1 (UCH-L1), have a significantly increased number of defective spermatozoa, suggesting that UCH-L1 functions in sperm quality control during epididymal maturation. The epididymis is the site of spermatozoa maturation, transport and storage. Region-specific functions along the epididymis are essential for establishing the environment required for sperm maturation. We analyzed the region-specific expression of UCH-L1 and UCH-L3 along the epididymis, and also assessed the levels of ubiquitin, which has specificity for UCH-L1. In wild-type mice, western blot analysis demonstrated a high level of UCH-L1 expression in the caput epididymis, consistent with ubiquitin expression, whereas UCH-L3 expression was high in the cauda epididymis. We also investigated the function of UCH-L1 and UCH-L3 in epididymal apoptosis induced by efferent duct ligation. The caput epididymides of* gad *mice were resistant to apoptotic stress induced by efferent duct ligation, whereas* Uchl3 *knockout mice showed a marked increase in apoptotic cells following ligation. In conclusion, the response of* gad *and* Uchl3 *knockout mice to androgen withdrawal suggests a reciprocal function of the two UCH enzymes in the caput epididymis.*
Key words: *apoptosis, epididymis, ubiquitin, UCH*

Introduction

The mammalian epididymis is a highly convoluted tubule that connects the efferent ducts of the testis to the vas deferens [2, 8]. The epididymis is composed of three distinct compartments, caput (head), corpus (body) and cauda (tail), each having a specific role in sperm maturation, sustenance, transport, and storage [2, 6]. However, the molecular basis for the maturation process remains largely unknown.

It has been suggested that the epididymis acts as a quality control organ to eliminate defective spermato-

(Received 12 August 2005 / Accepted 4 November 2005)
Address corresponding: K. Wada, Department of Degenerative Neurological Diseases, National Institute of Neuroscience, National Center of Neurology and Psychiatry, 4–1–1 Ogawahigashi-cho, Kodaira, Tokyo 187-8502, Japan

zoa before ejaculation [37]. The epididymis is an organ with voluminous protein traffic between the epithelium and lumen. Numerous proteins, secreted in an apocrine manner by the epididymal epithelium, are implicated in spermatozoa maturation [18]. Two major components of the ubiquitin-dependent proteolytic pathway, ubiquitin and UCH-L1 (PGP9.5), are expressed in epididymal tissue [10, 35]. Ubiquitin is present in human seminal plasma [26], and defective spermatozoa become ubiquitinated during epididymal passage [23, 37]. Our previous work showed that UCH-L1 associates with monoubiquitin and stabilizes its expression [31]. In addition, it has been suggested that UCH-L1 functions as a regulator of apoptosis via the ubiquitin pathway [13, 23, 25]. We found that testes of gracile axonal dystrophy (*gad*) mice, which lack UCH-L1, have reduced ubiquitin levels and are resistant to cryptorchid injury–mediated germ cell apoptosis [25]. Furthermore, our recent work demonstrated that the percentage of morphologically abnormal spermatozoa is significantly higher in *gad* mice, compared with wild-type mice [23].

Two mouse UCH isozymes, UCH-L1 and UCH-L3, are strongly but reciprocally expressed in the testis during spermatogenesis [25], suggesting that these proteins have distinct functions in the testis [23], even though they have high amino acid sequence identity and share significant structural similarity [21]. The functional regionalization of the epididymis is delineated at the molecular level by regional differences in gene expression [16–19]. Regional differences along the epididymis might be essential characteristics of the environment required for sperm quality control. Although it has been shown that UCH-L1 and UCH-L3 have reciprocal functions with respect to cryptorchid injury, their molecular functions in regulating sperm quality during epididymal passage are not fully understood. Thus, we examined the epididymal expression of UCH-L1 and UCH-L3 with regard to their involvement in the regulation of apoptosis. In addition, we assessed the reciprocal functions of these two proteins in the epididymis.

Materials and Methods

Animals

We used *gad* (CBA/RFM) [34] and *Uchl3* knockout (C57BL/6J) [21] male mice at 10 weeks of age. The *gad* mouse is an autosomal recessive mutant that was obtained by crossing CBA and RFM mice. The *gad* line has been maintained by intercrossing for more than 20 generations [34]. *Uchl3* knockout mice were generated by the standard method [21] using homologously recombinant ES cells, and the knockout line has been back-crossed several times to C57BL/6J mice. Both strains are maintained at our institute. Animal care and handling were in accordance with our institutional regulations for animal care and were approved by the Animal Investigation Committee of the National Institute of Neuroscience, National Center of Neurology and Psychiatry.

Unilateral efferent duct ligation

Animals were either left intact to serve as controls or were unilaterally ligated at the efferent duct [9, 38]. Four mice in each group were anesthetized with pentobarbital (Abbott Laboratories, North Chicago, IL), and the testis and epididymis on the right side were exposed through a scrotal incision. The thin avascular attachment joining the initial segment of the epididymis to the tunica albuginea was cut to permit exposure of the efferent ducts coursing above and parallel to the vascular supply. A silk suture was passed by needle through the thin sheet of connective tissue between the ductules and the blood vessels, and the efferent ducts were occluded by ligation. Mice were sacrificed 2 or 4 days after ligation. Both epididymides were immersed in 4% paraformaldehyde for at least 24 hr before they were dehydrated and embedded in paraffin [22].

Histological and immunohistochemical assessment of the epididymis

The caput, corpus and cauda epididymides along the epididymal region embedded in paraffin were cut into 4-μm sections and stained with hematoxylin and eosin. Light microscopy was used for routine observations. For immunohistochemical staining, the sections were incubated with 10% goat serum for 1 h at room temperature followed by incubation overnight at 4°C with a rabbit polyclonal antibody raised against peptides within UCH-L1 or UCH-L3 (1:1,000 dilution; peptide antibodies [24]) and ubiquitin (1:500; DakoCytomation, Glostrup, Denmark) in PBS containing 1% BSA. Sections were then incubated for 1 h with biotin-conjugated anti-rabbit IgG diluted 1:200 in PBS, followed by

Vectorstain ABC-PO (Vector Laboratories, Burlingame, CA) for 30 min at room temperature. Sections were developed using 3,3'-diaminobenzidine and counterstained with hematoxylin.

In situ apoptosis was detected by TUNEL (TdT-mediated nick end-labeling) staining with the DeadEnd Fluorometric TUNEL system (Promega, Madison, WI) according to the manufacturer's instructions, to identify apoptotic cells in situ via specific labeling of nuclear DNA fragmentation. Quantification was performed using four mice on each of postoperative days 0, 2 and 4. The total number of apoptotic cells was determined by counting the positively stained nuclei in each caput epididymis section [9]. Four sections from each mouse and 100 total circular tubules per group were processed.

Western blotting

Western blots were performed as previously reported [24]. Total protein (10 μg/lane) from each epididymal region including spermatozoa was subjected to SDS-polyacrylamide gel electrophoresis using 15% gels (Perfect NT Gel, DRC, Japan). Proteins were electrophoretically transferred to polyvinylidene difluoride membranes (Bio-Rad, Hercules, CA) and blocked with 5% non-fat milk in TBS-T (50 mM Tris base, pH 7.5, 150 mM NaCl, 0.1% (w/v) Tween-20). The membranes were incubated individually with primary antibodies to monoubiquitin (1:1,000; u5379, Sigma-Aldrich, St. Louis, MO), UCH-L1 and UCH-L3 (1:1,000 dilution; anti-peptide antibodies [24]), p53, Bax, and Bcl-xL (1:1,000 dilution; all from Cell Signaling Technology, Beverly, MA), and Bcl-2 (1:500; Transduction Laboratories, Franklin Lakes, NJ). Blots were further incubated with peroxidase-conjugated goat anti-mouse IgG or goat anti-rabbit IgG (1:5,000 dilution; Pierce, Rockford, IL) for 1 h at room temperature. Immunoreactions were visualized using SuperSignal West Dura Extended Duration Substrate (Pierce) and analyzed using a ChemiImager (Alpha Innotech, San Leandro, CA). Each protein level was normalized to α-tubulin following analysis with a ChemiImager using AlphaEase software.

Statistical analysis

The mean and standard deviation were calculated for all data (presented as mean ± SD). Student's *t*-test was used for statistical analysis.

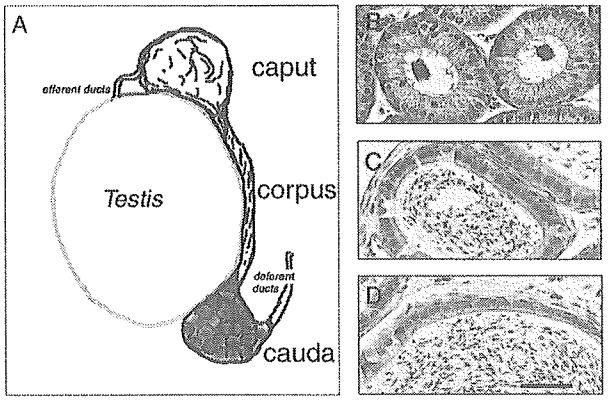

Fig. 1. A: Diagram of the epididymis. B–D: Morphology of the caput (B), corpus (C) and cauda (D) epididymidis from a wild-type mouse. Magnification, 200×. *Scale bar*, 40 μm.

Results

Levels of UCH-L1 and UCH-L3 in individual epididymal regions

The epididymis is a single long, coiled tubule situated on the surface of the testis (Fig. 1A). The epididymal epithelium is composed of four major cell types, principal cells, basal cells, clear cells and narrow cells [7], and can be divided anatomically and functionally into three regions, the caput, corpus and cauda epididymis (Fig. 1B, C, D). We used western blotting to characterize UCH-L1 and UCH-L3 levels along the epididymis (Fig. 2). In wild-type mice, the level of UCH-L1 was highest in the caput epididymis and that of UCH-L3 was highest in the cauda epididymis. UCH-L1 and UCH-L3 were not observed in *gad* and *Uchl3* knockout mice, respectively (Fig. 2; comparison of UCH-L1 and UCH-L3 levels with those in wild-type control mice).

Immunohistochemistry of UCH-L1, UCH-L3 and ubiquitin in the epididymis

Under light microscopy, granular and diffuse UCH-L1 and UCH-L3 immunoreactivity was detected in many epithelial cells of the caput, corpus and cauda epididymis in wild-type mice (Fig. 3A, C). Granular immunoreactivity to ubiquitin was seen in the epithelial cells of the epididymis (Fig. 3B). The distribution of ubiquitin in the corpus and cauda epididymal epithelial cells was similar to that of the caput epididymis,

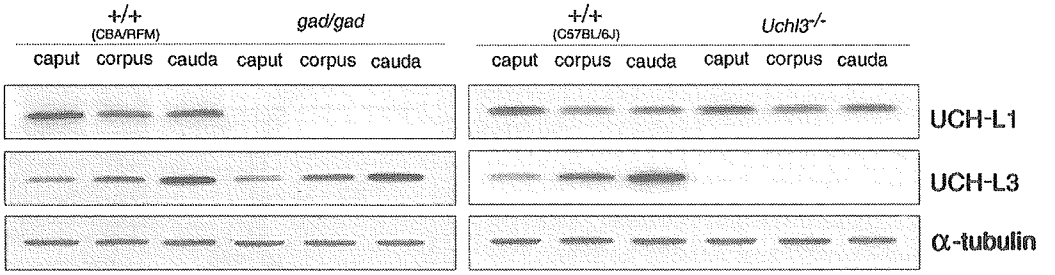

Fig. 2. Comparison of UCH-L1 and UCH-L3 expression by western blotting of caput, corpus and cauda epididymis lysates from two wild-type (CBA/RFM and C57BL/6J), *gad* and *Uchl3* knockout mice. Blots were reprobed for α-tubulin, which was used to normalize the protein load. Images are representative of four independent experiments.

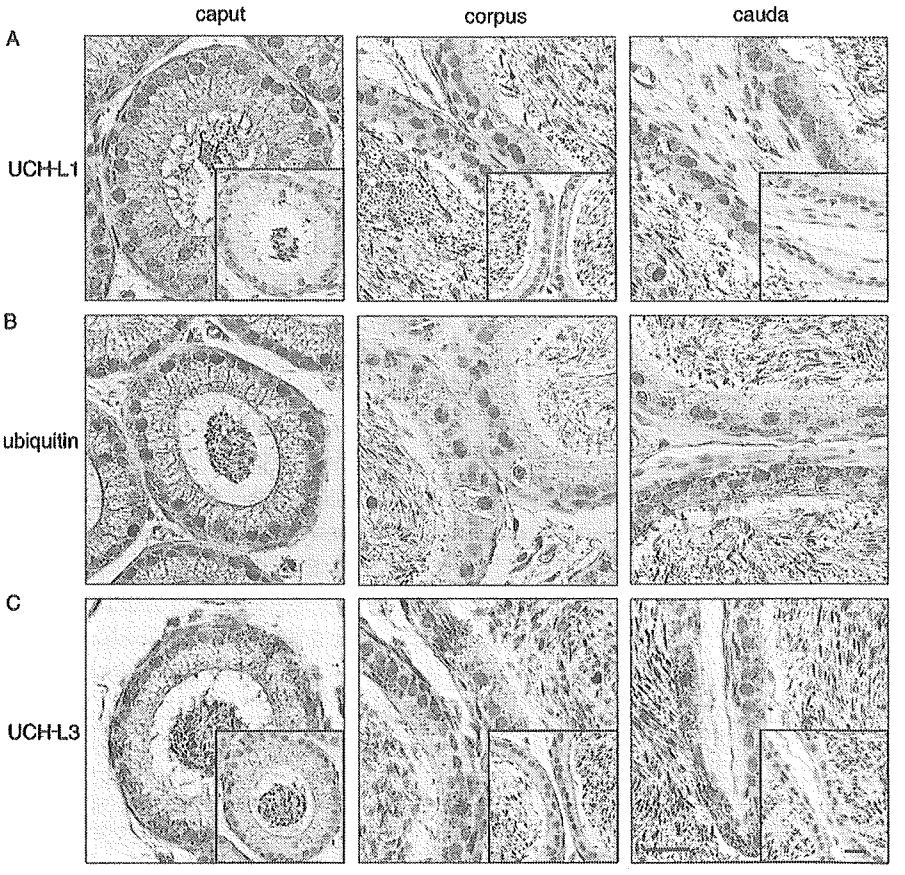

Fig. 3. Immunohistochemistry of UCH-L1, UCH-L3, and ubiquitin in the individual epididymal regions of wild-type mice. Each of the protein-positive cells in the caput, corpus and cauda epididymis is stained by DAB. The insets show that no cells are positive for UCH-L1 and UCH-L3 in the individual epididymal compartments from *gad* (A) and *Uchl3* knockout (C) mice, respectively. A: UCH-L1-positive cells. B: Ubiquitin-positive cells. C: UCH-L3-positive cells. Magnification, 400×. *Scale bar*, 20 μm.

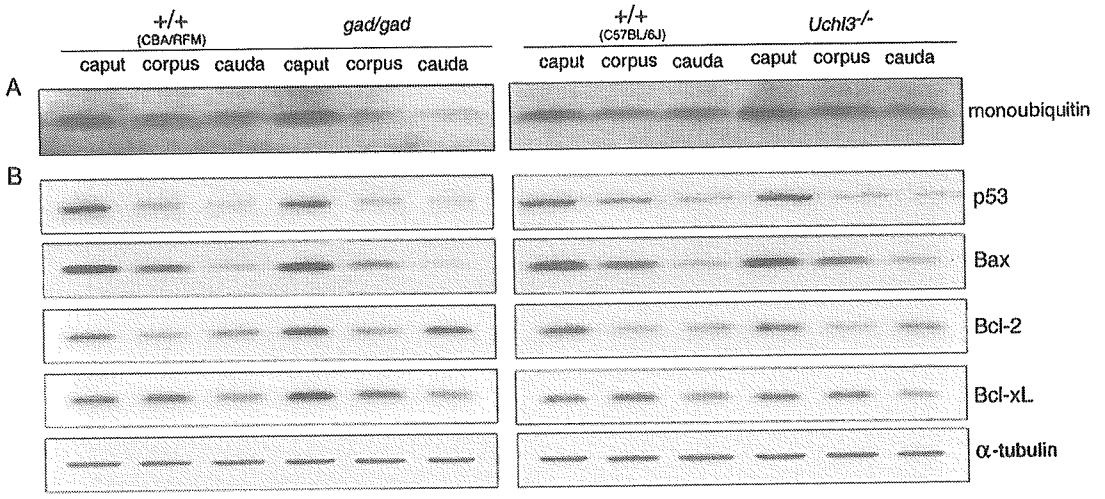

Fig. 4. Western blot analyses showing monoubiquitin and apoptotic proteins in the individual epididymal regions. Total protein (10 μg per lane) was prepared from the caput, corpus and cauda epididymidis from two wild-type (CBA/RFM and C57BL/6J), *gad* and *Uchl3* knockout mice. The blots show the expression levels of monoubiquitin (A) and apoptotic proteins (p53 and Bax) and antiapoptotic proteins (Bcl-2 and Bcl-xL) (B). Blots were reprobed for a-tubulin, which was used to normalize the protein load. Images are representative of four independent experiments.

the ubiquitin staining in these epididymal regions was less intense (Fig. 3B). Immunoreactivity to both UCH-L1 and ubiquitin was intense in the caput epididymal epithelial cells, which was consistent with the expression level (Fig. 2 and Fig. 4A). Diffuse cytoplasmic immunoreactivity in the epididymal epithelial cells to UCH-L3 was intense in the cauda epididymis (Fig. 3C). As shown previously [24], no UCH-L1 or UCH-L3 immunoreactivity was found in the epididymal epithelial cells of *gad* and *Uchl3* knockout mice, respectively (Fig. 3A, C. inset).

Region-specific localization of ubiquitin and apoptotic proteins in the caput epididymis

We previously reported that UCH-L1 binds ubiquitin, and that the level of ubiquitin is decreased in *gad* mice [25, 31]. To determine whether UCH-L1 is associated with the ubiquitin level in the epididymis, we performed western blot analysis of the individual epididymal regions. The monoubiquitin level was markedly higher in the caput epididymis than in the corpus and cauda epididymis, and the low level of monoubiquitin in *gad* mice is consistent with our previous report [25] (Fig. 4A). The epididymis of *Uchl3* knockout mice did not show a difference in ubiquitin level compared with the corresponding wild-type controls.

To explore whether apoptotic phenomenon of spermatozoa in the caput epididymis is in accord with the high expression of apoptotic proteins, we used western blot analysis to verify the expression levels of p53 and Bcl-2 family proteins, which are associated with cell death [12, 28, 29]. The levels of p53 and Bax protein, considered to be proapoptotic, were strikingly high in the caput epididymis, consistent with the pattern of the monoubiquitin level (Fig. 4B). In the *gad* mouse, the levels of the antiapoptotic proteins, Bcl-2 and Bcl-xL, were markedly elevated compared in wild-type mice in the caput epididymis [23] as well as a possible increase in the corpus and cauda epididymis, whereas the levels of apoptotic proteins, p53 and Bax, were unchanged (Fig. 4B). However, we did not detect a difference in the analyzed protein levels between the epididymis of *Uchl3* knockout and wild-type mice.

Region-specific apoptosis in the epididymis following unilateral efferent duct ligation

Androgen deprivation by efferent duct ligation induces glandular epithelial cell death via an apoptotic mechanism [9, 38]. We previously showed that germ cell apoptosis differs between *gad* and *Uchl3* knockout mice following cryptorchid injury [25]. To detect apoptosis in the epididymis following efferent duct li-

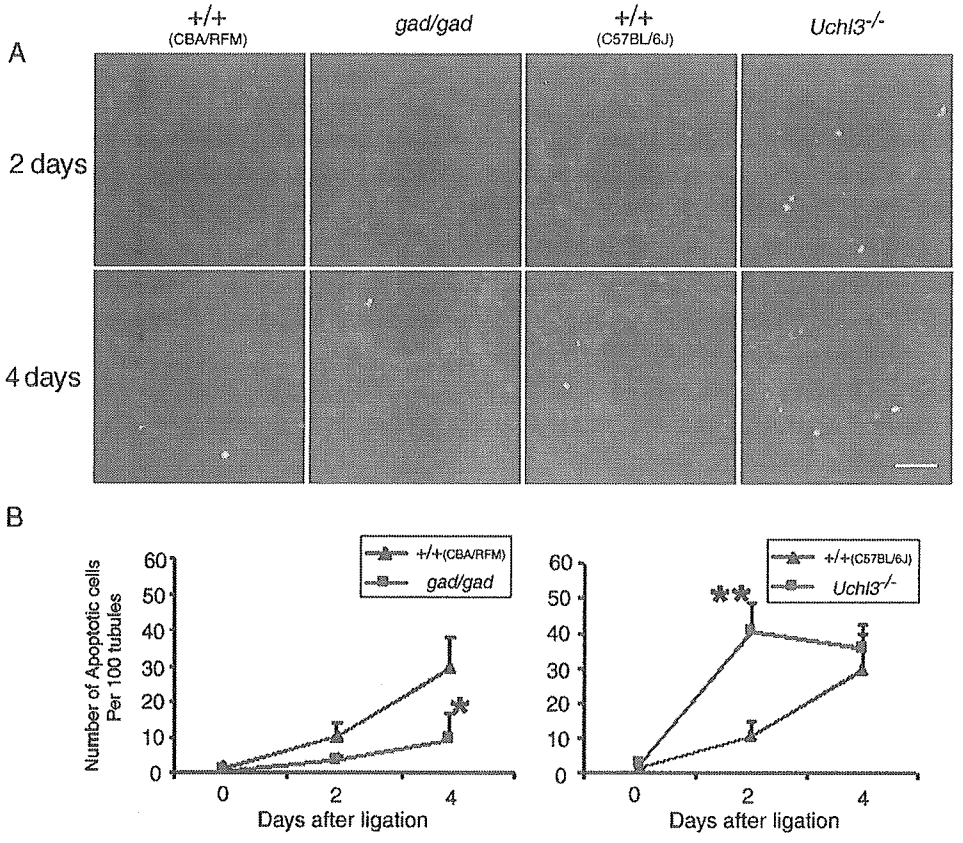

Fig. 5. TUNEL staining of apoptotic cells in the caput epididymis following unilateral efferent duct ligation. A: TUNEL staining in the caput epididymis cross-sections on days 2 and 4 after ligation. Green fluorescence, TUNEL-positive cells; red fluorescence, nuclei stained with propidium iodide. Magnification, 200×. *Scale bar*, 30 μm. B: Quantitation of epithelial cell apoptosis in the caput epididymis following efferent duct ligation. The number of apoptotic epithelial cells in *gad* and wild-type mice is shown on the left. Each value represents the mean ± SD; $^{*}P<0.05$. The number of apoptotic epithelial cells in *Uchl3* knockout and wild-type mice is shown on the right. Each value represents the mean ± SD; $^{**}P<0.01$.

gation, we used an *in situ* TUNEL assay to examine apoptosis in *gad* and *Uchl3* knockout mice on postoperative days 2 and 4 (Fig. 5). After efferent duct ligation, epithelial cell apoptosis was observed only in the caput epididymis (mostly the initial segment). The caput epididymis showed a time-dependent increase in epithelial cell apoptosis after efferent duct ligation and epithelial cell apoptosis was found mainly in the principal cells (Fig. 5A). Compared with wild-type mice, the caput epididymis of *Uchl3* knockout mice showed a marked increase in apoptotic epithelial cells on postoperative day 2, whereas *gad* mice resisted efferent duct-ligated epithelial cell apoptosis (Fig. 5A). By postoperative day 2, the number of apoptotic cells per 100 tubules increased with statistical significance ($^{**}P<0.01$, $n=4$) in the caput epididymis of *Uchl3* knockout mice as compared with wild-type mice (Fig. 5B). However, *gad* mice showed resistance to ligation-induced apoptosis in the caput epididymis relative to wild-type mice by postoperative day 4 ($^{*}P<0.05$, $n=4$) (Fig. 5B).

Discussion

After leaving the testis via the testicular rete, spermatozoa collect in the epididymis, where they undergo final maturation and storage [2, 36, 37]. During epididymal passage, ubiquitination may trigger apoptotic mechanisms that recognize and eliminate abnormal sper-

matozoa, and ubiquitination is believed to play an important role in controlling sperm quality to ensure the production of intact, functional spermatozoa [10, 27, 37]. Ubiquitination of abnormal spermatozoa predominantly occurs in the caput epididymis [37].

Previous studies have shown that two closely-related UCH isozymes, UCH-L1 and UCH-L3 have distinct expression patterns during spermatogenesis [24] and reciprocal functions following cryptorchid injury [25]. We have proposed that UCH-L1 might function as a regulator of apoptosis. Indeed, UCH-L1-deficient *gad* mice are resistant to apoptotic stress [13, 23, 25], and this apoptotic resistance leads to alterations in sperm motility and morphology as well as an increased number of defective spermatozoa in the epididymis of *gad* mice [23]. Our present study demonstrated that UCH-L1 and UCH-L3 have distinct expression patterns along the epididymis in wild-type mice (Fig. 2). We detected a high level of UCH-L1 in the caput epididymis, the main maturation organ, whereas the UCH-L3 level was high in the cauda epididymis, the main storage organ [10]. These region-specific variations in UCH-L1 and UCH-L3 level suggest that they have different functions in the epididymis. The regional differentiation of the epididymis, as suggested by region-specific gene expression, reflects different luminal environments between the regions [16, 19].

We also determined the expression pattern/level of the major component of the proteolytic pathway, ubiquitin, which has specificity for UCH-L1. UCH-L1 associates with monoubiquitin [31], and the monoubiquitin level is reduced in *gad* mice relative to wild-type mice [25, 31]. Predictably, monoubiquitin expression pattern showed similar patterns to UCH-L1 and the monoubiquitin level was reduced in the epididymis of *gad* mice, which had its highest level in the caput epididymis relative to the corpus or cauda epididymis in wild-type mice (Figs. 3 and 4A). Ubiquitin induction is important for regulating programmed cell death, which is a fundamental component of spermatogenesis [1, 23, 32]. Under specific circumstances, the caput epididymis contains a high level of ubiquitin, which may serve to maintain apoptotic mechanisms that eliminate abnormal spermatozoa [37]. This is consistent with the high levels of apoptotic p53 and Bax observed in the caput epididymis compared with the corpus and cauda epididymis (Fig. 4B). Protein p53 and Bax are classically thought to be involved in regulating apoptotic processes, and are targets for ubiquitination [5, 7, 29, 30]. The role of p53 in mediating apoptosis in the male genital tract has been demonstrated in several mice lines [28, 29, 42]. However, p53-independent apoptosis is suggested in the prostate and seminal vesicles by androgen withdrawal or in the rat epididymis by deprivation of luminal factors [3, 11, 14, 38]. Previous studies indicated that Bcl-2 family proteins are involved in the induction or prevention of apoptosis [12, 33, 39, 40]. In *gad* mice, in the present study, the levels of the antiapoptotic proteins, Bcl-2 and Bcl-xL, were markedly increased in the caput epididymis (Fig. 4B), although there was no difference in the levels of the apoptotic proteins, p53 and Bax, relative to wild-type mice. The high levels of Bcl-2 and Bcl-xL in the caput epididymis of *gad* mice is consistent with a previous report that the percentage of morphologically abnormal spermatozoa is significantly higher in *gad* mice [23]. Therefore, the variations of in the levels of Bax, and Bcl-2 and Bcl-xL combined in the caput epididymis probably maintain the regulation of apoptosis [4].

Our previous work focused on the reciprocal functions that UCH-L1 and UCH-L3 exhibit, a distinct feature in testicular germ cells following cryptorchid-induced apoptosis [25]. To characterize the distinct functions of UCH-L1 and UCH-L3 in the epididymis, *gad* and *Uchl3* knockout mice were examined after efferent duct ligation. The epididymal epithelium of the two mutant mice showed differences in apoptotic induction following efferent duct ligation (Fig. 5), after which the circulating androgen level decreases rapidly as a result of apoptotic cell death [9, 20, 38]. After duct ligation, the number of apoptotic cells increased in the caput epididymis of *Uchl3* knockout mice compared with wild-type mice, whereas *gad* mice showed relative resistance in this regard (Fig. 5B). In *gad* mice, the resistance to apoptotic stress can be explained by the high levels of Bcl-2 and Bcl-xL combined in the caput epididymis (Fig. 4B). The tissue androgen level is higher in the caput epididymis than in the corpus or cauda epididymis [15, 38]; thus, apoptotic cells showed in the caput epididymis rather than in the corpus and cauda epididymis following efferent duct ligation. These results may suggest that UCH-L1 and UCH-L3 have reciprocal functions in the caput epididymis fol-

lowing apoptotic stress induced by androgen withdrawal, as was shown with cryptorchid stress [25].

We cannot explain the profound apoptotic phenomenon observed in the present study in the caput epididymis of *Uchl3* knockout mice after efferent duct ligation by the balance of the Bcl-2 family proteins alone. Although our previous report showed that the Nedd8 expression level increased in the testis of *Uchl3* knockout mice [25], we found no difference in the present study (data not shown). The mechanism with regard to the antiapoptotic function of UCH-L3 requires further study. Our present study demonstrated that UCH-L1 and UCH-L3 have distinct expression levels along the epididymis as well as reciprocal functions in response to apoptotic stress induced by androgen withdrawal.

Acknowledgments

We thank H. Kikuchi for technical assistance with tissue sections, and M. Shikama for the care and breeding of animals.

Grant support: This work was supported by Grants-in-Aid for Scientific Research from the Ministry of Health, Labour and Welfare of Japan, Grants-in-Aid for Scientific Research from the Ministry of Education, Culture, Sports, Science and Technology of Japan, a grant from the Pharmaceuticals and Medical Devices Agency of Japan, and a grant from Japan Science and Technology Agency. This paper was supported (in part) by research funds of Chonbuk National University in 2005.

References

1. Baarends, W.M., van der Laan, R., and Grootegoed, J.A. 2000. Specific aspects of the ubiquitin system in spermatogenesis. *J. Endocrinol. Invest.* 23: 597–604.
2. Bedford, J.M. 1979. pp. 7–21. *In*: Evolution of the sperm maturation and sperm storage functions of the epididymis,The Spermatozoon (Bedford DWFaJM, ed). Urban and Schwarzenberg Inc., Baltimore-Muunich.
3. Berges, R.R., Furuya, Y., Remington, L., English, H.F., Jacks, T., and Isaacs, J.T. 1993. Cell proliferation, DNA repair, and p53 function are not required for programmed death of prostatic glandular cells induced by androgen ablation. *Proc. Natl. Acad. Sci. USA.* 90: 8910–8914.
4. Borner, C. 2003. The Bcl-2 protein family: sensors and checkpoints for life-or-death decisions. *Mol. Immunol.* 39: 615–647.
5. Chipuk, J.E. and Green, D.R. 2004. Cytoplasmic p53: Bax and Forward. *Cell Cycle* 3: 429–431.
6. Cooper, T.G. 1998. pp. 602–609. *In*: Epididymis, Encyclopedia of Reproduction (Neil EKaJD, ed). Academic Press Inc., San Diego.
7. Dimmeler, S., Breitschopf, K., Haendeler, J., and Zeiher, A.M. 1999. Dephosphorylation targets Bcl-2 for ubiquitin-dependent degradation: a link between the apoptosome and the proteasome pathway. *J. Exp. Med.* 189: 1815–1822.
8. Ezer, N. and Robaire, B. 2003. Gene expression is differentially regulated in the epididymis after orchidectomy. *Endocrinology* 144: 975–988.
9. Fan, X. and Robaire, B. 1998. Orchidectomy induces a wave of apoptotic cell death in the epididymis. *Endocrinology* 139: 2128–2136.
10. Fraile, B., Martin, R., De Miguel, M.P., Arenas, M.I., Bethencourt, F.R., Peinado, F., Paniagua, R., and Santamaria, L. 1996. Light and electron microscopic immunohistochemical localization of protein gene product 9.5 and ubiquitin immunoreactivities in the human epididymis and vas deferens. *Biol. Reprod.* 55: 291–297.
11. Furuya, Y., Lin, X.S., Walsh, J.C., Nelson, W.G., and Isaacs, J.T. 1995. Androgen ablation-induced programmed death of prostatic glandular cells does not involve recruitment into a defective cell cycle or p53 induction. *Endocrinology* 136: 1898–1906.
12. Gross, A., McDonnell, J.M., and Korsmeyer, S.J. 1999. BCL-2 family members and the mitochondria in apoptosis. *Genes. Dev.* 13: 1899–1911.
13. Harada, T., Harada, C., Wang, Y.L., Osaka, H., Amanai, K., Tanaka, K., Takizawa, S., Setsuie, R., Sakurai, M., Sato, Y., Noda, M., and Wada, K. 2004. Role of ubiquitin carboxy terminal hydrolase-L1 in neural cell apoptosis induced by ischemic retinal injury *in vivo*. *Am. J. Pathol.* 164: 59–64.
14. Jara, M., Esponda, P., and Carballada, R. 2002. Abdominal temperature induces region-specific p53-independent apoptosis in the cauda epididymidis of the mouse. *Biol. Reprod.* 67: 1189–1196.
15. Jean-Faucher, C., Berger, M., Gallon, C., de Turckheim, M., Veyssiere, G., and Jean, C. 1986. Regional differences in the testosterone to dihydrotestosterone ratio in the epididymis and vas deferens of adult mice. *J. Reprod. Fertil.* 76: 537–543.
16. Jervis, K.M. and Robaire, B. 2001. Dynamic changes in gene expression along the rat epididymis. *Biol. Reprod.* 65: 696–703.
17. Jervis, K.M. and Robaire, B. 2002. Changes in gene expression during aging in the Brown Norway rat epididymis. *Exp. Gerontol.* 37: 897–906.
18. Kirchhoff, C. 1998. Molecular characterization of epididymal proteins. *Rev. Reprod.* 3: 86–95.
19. Kirchhoff, C. 1999. Gene expression in the epididymis. *Int. Rev. Cytol.* 188: 133–202.
20. Knorr, D.W., Vanha-Perittula, T., and Lipsett, M.B. 1970. Structure and function of rat testis through pubescence. *Endocrinology* 86: 1298–1304.
21. Kurihara, L.J., Semenova, E., Levorse, J.M., and Tilghman,